Research Square

Preprints are preliminary reports that have not undergone peer review.
They should not be considered conclusive, used to inform clinical practice,
or referenced by the media as validated information.

Engineered Exosomes Delivering FOSB siRNA Alleviate Podocyte Injury in Hepatitis B Virus-Associated Nephritis

Jie Li
The Affiliated Hospital of Qingdao University
Yongzheng Hu
The Affiliated Hospital of Qingdao University
Xinyi Hao
The Affiliated Hospital of Qingdao University
Yabin Wang
The Affiliated Hospital of Qingdao University
Wei Jiang
jiangwei866@qdu.edu.cn
The Affiliated Hospital of Qingdao University

Research Article

Keywords: Hepatitis B virus-associated glomerulonephritis, Hepatitis B virus X protein, Engineered exosomes, FOSB, Small interfering RNA

Posted Date: November 19th, 2026

DOI: https://doi.org/10.21203/rs.3.rs-11410819/v1

License: This work is licensed under a Creative Commons Attribution 4.0 International License.
Read Full License

Additional Declarations: No competing interests reported.

Engineered Exosomes Delivering FOSB siRNA Alleviate Podocyte Injury in Hepatitis B Virus-Associated Nephritis

Jie Li,Master of Science,Nephrology Department,The Affiliated Hospital of Qingdao University, Shandong Province, China,1474413983@qq.com
Yongzheng Hu,Doctor of Medicine,Nephrology Department,The Affiliated Hospital of Qingdao University, Shandong Province, China,hu_yongzheng_med@126.com
Xinyi Hao,Master of Science,Nephrology Department,The Affiliated Hospital of Qingdao University, Shandong Province, China,haoxinyi@qdu.edu.cn
Yabin Wang,Master of Science,Nephrology Department,The Affiliated Hospital of Qingdao University, Shandong Province, China,13869627306@163.com
Wei Jiang,Doctor of Medicine,Nephrology Department,The Affiliated Hospital of Qingdao University, Shandong Province, China,jiangwei866@qdu.edu.cn(Corresponding Author)

Abstract

Hepatitis B virus-associated glomerulonephritis (HBV-GN) is the common extrahepatic manifestation of HBV infection and a major secondary glomerular disease in China. Upregulated FOSB mediates podocyte injury induced by HBx, whereas silencing FOSB can reverse this pathological change. Bone marrow mesenchymal stem cell-derived exosomes (BMSC-Exos) exhibit excellent biocompatibility, while their clinical application is limited by short circulating half-life and insufficient drug loading capacity. Herein, we constructed Cyclo(RGDfC)-modified BMSC-Exos encapsulated with FOSB siRNA and investigated its therapeutic potential against HBx-mediated podocyte damage. Transcriptomic analysis of renal samples from HBV-GN patients and healthy volunteers screened FOSB as a key pathogenic gene. We established an in vitro HBx-overexpressing podocyte model and an in vivo HBx transgenic mouse model. Engineered exosomes were prepared via covalent coupling of Cyclo(RGDfC) and siRNA loading, followed by comprehensive characterization. Our data verified that HBx induced FOSB overexpression. Cyclo(RGDfC)-modified engineered exosomes can be internalized by podocytes. Relative to unmodified exosomes, these constructs significantly downregulated FOSB, alleviated podocyte apoptosis and inflammatory response, and ameliorated renal lesions and dysfunction in transgenic mice. Collectively, Cyclo(RGDfC)-modified FOSB siRNA-loaded BMSC-Exos hinder HBV-GN progression through inhibiting FOSB-dependent podocyte injury, which represents a prospective therapeutic strategy for HBV-GN.

Keywords: Hepatitis B virus-associated glomerulonephritis; Hepatitis B virus X protein; Engineered exosomes; FOSB; Small interfering RNA

Introduction

Hepatitis B virus (HBV) infection remains a leading contributor to global liver-related morbidity and mortality[1]. Beyond hepatic lesions, HBV triggers a wide spectrum of extrahepatic manifestations, among which hepatitis B virus-associated glomerulonephritis (HBV-GN) ranks as the most prevalent renal complication[2]. The pathogenesis of HBV-GN is multifactorial. Circulating immune complexes formed after HBV infection deposit within glomeruli, activate the complement cascade and initiate local inflammatory infiltration[3]. Meanwhile, direct viral invasion of renal tubular epithelial cells and subsequent podocyte injury synergistically drive disease progression[4, 5]. The HBV genome encodes four open reading frames, and the X region

generates HBx, a 154-amino-acid multifunctional regulatory protein that modulates DNA damage, inflammatory response, cell proliferation and oxidative stress[6]. In the cytoplasm, HBx activates multiple signaling cascades to facilitate HBV replication; in the nucleus, it binds covalently closed circular DNA of HBV and recruits diverse transcription factors and epigenetic regulators to amplify viral promoter activity[7]. Accumulating transfection experiments demonstrate that HBx dysregulates cyclin expression to manipulate apoptosis and cell cycle progression in tubular epithelial cells and podocytes[8, 9]. Additionally, HBx activates the NF-κB pathway to promote renal epithelial-mesenchymal transition and inflammation in human proximal tubular cells[10], collectively confirming the central pathogenic role of HBx in HBV-GN.

Mesenchymal stem cells (MSCs) are self-renewable multipotent adult stem cells isolated from bone marrow, adipose tissue, umbilical cord and placenta[11]. MSCs exert therapeutic effects mainly via paracrine signaling mediated by exosomes. Exosomes are lipid bilayer vesicles ranging from 30 to 150 nm, packed with functional proteins, lipids, mRNA and miRNA to modulate proliferation, apoptosis and inflammation of recipient cells[12]. MSC-derived exosomes (MSC-Exos) alleviate acute kidney injury and chronic kidney disease by suppressing inflammation, oxidative stress, apoptosis and renal fibrosis[13-15]. Nevertheless, native exosomes are hindered by short blood circulation half-life, inconsistent cellular source quality and limited drug loading capacity for clinical translation. Engineered exosomes fabricated via bioengineering overcome these drawbacks by stabilizing cargo molecules, improving bioavailability, reducing systemic toxicity and achieving targeted tissue accumulation[16].

Podocytes constitute the core component of the glomerular filtration barrier, where integrins mediate podocyte anchorage to the glomerular basement membrane. Integrin αvβ3, a heterodimeric transmembrane receptor abundant on podocytes, maintains normal cellular adhesion and cytoskeletal homeostasis; its aberrant activation correlates with foot process effacement and proteinuria under pathological conditions. Cyclo(RGDfC), a five-amino-acid cyclic peptide, serves as a classic targeting ligand for gene and drug delivery by specifically binding integrin αvβ3 and competitively inhibiting endogenous ligands such as fibronectin and vitronectin[17, 18]. Prior studies validate the renal-targeting capability of Cyclo(RGDfC)-modified nanocarriers: peptide-conjugated quantum dots selectively bind and internalize into primary podocytes and isolated glomeruli via αvβ3[19]; RGD-functionalized liposomes accumulate in fibrotic kidneys to mitigate glomerular inflammation without obvious systemic toxicity[20]; polymer nanoparticles modified with Cyclo(RGDfC) deliver miRNA-30a to podocytes and attenuate podocyte damage and glomerulosclerosis[21]. These findings support Cyclo(RGDfC) as an ideal ligand for podocyte-targeted therapy.

Our previous transcriptomic profiling of renal biopsies from HBV-GN patients revealed remarkable enrichment of the IL-17 signaling pathway and specific upregulation of FOSB, and further verified elevated FOSB expression concurrent with HBx-mediated podocyte injury. On this basis, we constructed Cyclo(RGDfC)-modified bone marrow MSC-exosomes loaded with FOSB siRNA. The present study aims to systematically investigate the protective efficacy and underlying molecular mechanisms of this engineered exosome against HBx-triggered podocyte damage and renal lesions in transgenic mice, offering an innovative cell-free therapeutic candidate for HBV-GN.

Materials and Methods

2.1 Human Specimens

Renal biopsy archival specimens from the Affiliated Hospital of Qingdao University were enrolled in this study, including 3 cases of HBV-GN and 3 healthy controls. Diagnoses were performed in accordance with the Guidelines for the Prevention and Treatment of Chronic Hepatitis B (2022 Edition) and KDIGO Clinical Practice Guidelines for Glomerular Diseases. All de-identified specimens were preserved from previous clinical diagnosis and treatment without additional sampling or clinical intervention, so informed consent was waived. This study was approved by the Ethics Committee of the Affiliated Hospital of Qingdao University (Ethics Approval No. QYFY WZLL 30952).

2.2 Establishment of Animal Models

Male HBx-transgenic C57BL/6 mice (5–6 weeks old) were gifted by a professor at the Korea Research Institute of Bioscience and Biotechnology. Age-matched wild-type male C57BL/6 mice were purchased from Beijing Vital River Laboratory Animal Technology Co., Ltd. All mice were housed in a specific pathogen-free (SPF) laboratory under a 12 h light/12 h dark cycle at (23±2) °C with a relative humidity of (50±5)%. Food and water were provided ad libitum. All animal experimental protocols were reviewed and approved by the Medical Ethics Committee of the Affiliated Hospital of Qingdao University, and all operations strictly complied with animal ethical guidelines. After one week of adaptive feeding, two independent in vivo animal experiments were conducted separately with isolated housing and processing.

2.2.1 In Vivo Assay of AAV-Mediated FOSB Knockdown

Wild-type C57BL/6 mice were assigned as the blank control group (Con group, n=3). HBx-transgenic mice were randomly divided into three groups via random number table (n= 3 per group): HBx group, HBx+AAV-shNC negative control group, and HBx+AAV-shFOSB intervention group. Each mouse received a tail vein injection of 100 μL corresponding viral vector at a dose of 5×10^{11} vg per mouse. Wild-type mice were injected with an equal volume of normal saline via tail vein, and all mice were raised for a 2-week intervention period.

2.2.2 In Vivo Intervention Assay of cRGD-Targeted Exosomes Loaded with si-FOSB

Another batch of wild-type C57BL/6 mice served as blank controls (Con group, n=6). HBx-transgenic mice were randomly divided into four groups (n=6 per group): HBx group, HBx+Exo group, HBx+cRGD-Exo/si-NC group, and HBx+cRGD-Exo/si-FOSB group. Mice in the Con and HBx groups received an equal volume of sterile PBS via tail vein, while the other groups were injected with corresponding exosomes at a single dose of 10 μg once every 3 days for a total 3-week treatment period.

At the end of both intervention cycles, all mice were fasted for 12 h and anesthetized via intraperitoneal injection of 1% sodium pentobarbital (50 mg/kg). Blood was collected via eyeball enucleation, followed by euthanasia through cervical dislocation. Bilateral kidneys were rapidly dissected. Fresh renal tissues were divided into two parts: one was fixed in 4% paraformaldehyde for pathological morphological detection, and the other was immediately stored at −80 °C for subsequent molecular biological assays.

2.3 Cell Culture, Transfection and Treatment

Immortalized human podocytes (HPCs, GD-C8618339) were obtained from Huizhiheyuan Biotechnology (China). HPCs were cultured in RPMI-1640 medium supplemented with 10% fetal bovine serum (FBS) and 100 U/mL penicillin/streptomycin. Cells were maintained at 33 °C in a humidified incubator with 5% CO_2. When cell density reached 70%, HPCs were shifted to 37 °C with 5% CO_2 for 10–14 days to complete differentiation. All subsequent intervention experiments

were performed using mature differentiated HPCs. Two independent in vitro intervention systems with distinct cell grouping strategies were set up as follows.

2.3.1 Grouping for HBx Lentivirus Infection Combined with FOSB Silencing

HPCs were randomly divided into four groups: Con group (cells cultured under routine passage without extra treatment as blank control); HBx group (5×10^5 HPCs infected with HBx lentivirus at a titer of 5×10^8 TU/mL at MOI=20 to construct HBx-stably expressing cell line); HBx+si-NC group (HBx-stable HPCs transfected with 50 nM negative control siRNA as negative control); HBx+si-FOSB group (HBx-stable HPCs transfected with 50 nM FOSB siRNA to induce FOSB knockdown).

2.3.2 Grouping for cRGD-Modified Exosome-Mediated FOSB Silencing

To investigate the therapeutic effect of cRGD-modified BMSC-derived exosomes delivering FOSB siRNA on HBx-expressing hepatic progenitor cells, stably HBx-transfected HPCs were seeded and randomly divided into four groups with different interventions. In the HBx+PBS group, cells were treated with 10 μL of sterile PBS buffer. In the HBx+Exo group, cells were incubated with 10 μL of unmodified BMSC-derived exosome suspension at a working concentration of 30 μg/mL. In the HBx+cRGD-Exo/si-NC group, cells were incubated with 10 μL of cyclic (RGDfC)-modified exosome suspension (30 μg/mL) preloaded with negative control siRNA, yielding a final siRNA concentration of 50 nM in the culture system. In the HBx+cRGD-Exo/si-FOSB group, cells were incubated with 10 μL of cyclic (RGDfC)-modified exosome suspension (30 μg/mL) preloaded with FOSB-specific siRNA at a final concentration of 50 nM. All interventions were performed in triplicate, and cells were harvested at the indicated time points for subsequent analyses.

2.4 Quantitative Real-Time PCR (qRT-PCR)

Total RNA was extracted using TRIzol reagent (Convoy Century, CW0580S) according to the manufacturer's instructions. Complementary DNA (cDNA) was synthesized with Evo M-MLV reverse transcription kit (Acres Bio, AG11706). qRT-PCR was carried out on a fluorescence quantitative PCR instrument using SYBR Green Pro Taq HS premixed kit (Acres Bio, AG11701), with GAPDH as the internal reference. Relative gene expression was calculated via the $2^{-}\Delta\Delta Ct$ method. Primer sequences are listed in Table 1.

Table 1 Primer sequences

Names	Sequences (5′–3′)
FOSB	ATCGACTTCAGGCGGAAACTG
GAPDH	GGTGAAGGTCGGTGTGAACG

2.5 Western Blot Analysis

Total protein was extracted from cells and renal tissues, and protein concentration was quantified using the BCA protein assay kit (Beyotime, P0012, Shanghai, China). Equal amounts of total protein were separated by 6%–12% SDS-PAGE and transferred onto 0.22 μm polyvinylidene difluoride (PVDF) membranes. Membranes were incubated with primary antibodies followed by corresponding secondary antibodies. Target bands were visualized with ECL chemiluminescence kit (Servicebio, G2014, Wuhan, China), and band gray values were quantified with ImageJ software. Antibodies used were as follows: HRP-conjugated goat anti-rabbit IgG (1:10,000, ZSGB-BIO, ZB-2301, Beijing, China); HRP-conjugated goat anti-mouse IgG (1:10,000,

ZSGB-BIO, ZB-2305, Beijing, China); anti-GAPDH (1:50,000, Proteintech, 60004-1-IG, USA); anti-FOSB (1:1,000, ABclonal, A19696); anti-H3 (1:10,000, Proteintech, 68345-1-IG, USA); anti-p-H3 (1:10,000, Proteintech, 66863-1-IG, USA); anti-Caspase3 (1:3,000, Proteintech, 66470-2-IG, USA); anti-β-actin (1:20,000, Proteintech, 66009-1-Ig, USA).

2.6 Cell Viability Assay

Cell viability was determined using the Cell Counting Kit-8 (CCK-8; Servicebio, Wuhan, China). Treated HPCs were resuspended at 1×10^5 cells/mL and seeded into 96-well plates. After incubation for 24, 48, 72 and 96 h, 10 μL CCK-8 solution was added to each well, followed by an additional 4 h incubation at 37 °C. Absorbance (OD value) at 450 nm was measured with a microplate reader (Thermo Fisher, USA).

2.7 ELISA Assay

Cell culture supernatants of HPCs were collected. The concentrations of IL-1β, IL-18 and TNF-α were detected using corresponding commercial ELISA kits (F0179 for IL-1β, F0138 for IL-18, F0121 for TNF-α, Shanghai Fanke Industrial Co., Ltd.) strictly following the manufacturer's protocols.

2.8 Transwell Invasion Assay

HPCs from each group were resuspended in serum-free medium and seeded into the upper chambers of Matrigel-precoated Transwell inserts (Corning, 3422). Complete medium containing 10% FBS was added to the lower chambers as chemoattractant. After 24 h incubation at 37 °C, non-invasive cells on the upper membrane surface were wiped off. Membranes were fixed with 4% paraformaldehyde and stained with crystal violet. Random fields were captured under a microscope to count invasive cells and compare cell invasive capacity across groups.

2.9 Flow Cytometry for Apoptosis Detection

HPCs were digested with EDTA-free trypsin, harvested, washed and resuspended. Cells were double-stained with Annexin V-FITC/7-AAD kit (Meilunebio, MA0429) in the dark according to instructions. Apoptosis ratio was immediately detected by flow cytometry, and the proportions of early apoptotic, late apoptotic and total apoptotic cells were analyzed with supporting software for statistical comparison.

2.10 Hematoxylin and Eosin (HE) Staining

Renal tissues fixed in 4% paraformaldehyde for 24 h were embedded in paraffin and cut into 4 μm-thick sections. HE staining was performed using commercial HE staining kit (Abcam, ab245880) following the manufacturer's manual. Slides were observed under an optical microscope (Nikon Eclipse Ci-L, Japan).

2.11 Immunohistochemistry and Immunofluorescence Staining

Paraffin renal sections were deparaffinized in xylene, rehydrated via graded ethanol, and blocked with 5% BSA at room temperature. For immunohistochemistry, sections were incubated with anti-F4/80 primary antibody at 4 °C overnight, followed by goat anti-mouse IgG secondary antibody at room temperature for 30 min. DAB color development was performed, and nuclei were counterstained with hematoxylin. Positive staining areas were quantified with ImageJ software under light microscopy. For immunofluorescence staining, sections were incubated with primary antibodies including anti-FOSB (1:200, Abcam), anti-nephrin (1:100, Boster Biotechnology, China) and anti-desmin (1:100, Boster Biotechnology, China). After PBS washing, sections were incubated with goat anti-mouse IgG secondary antibody. Nuclei were stained with DAPI, and images were captured with a fluorescence microscope.

2.12 Renal Function Detection

Mouse blood samples were centrifuged at 3000 r/min for 10 min at 4 °C to collect serum. Urine samples were centrifuged at 3000 × g for 10 min to remove precipitates. Serum urea nitrogen (BUN) and serum creatinine (Scr) levels were measured using corresponding detection kits (Nanjing Jiancheng Bioengineering Institute, Nanjing, China) per manufacturer's instructions. Twenty-four-hour urinary protein levels were quantified with urine protein assay kit (G4328, Servicebio, Wuhan, China).

2.13 Isolation, cRGD modification, FOSB siRNA loading, purification, and characterization of BMSC-derived exosomes

Bone marrow mesenchymal stem cells (BMSCs,CP-M131, Procell, Wuhan, China)) were cultured at 37 °C in a humidified atmosphere containing 5% CO2. When the cultures reached approximately 60–70% confluence, the cells were washed with PBS and maintained for 48 h in DMEM complete medium supplemented with 10% exosome-depleted serum. The conditioned medium was collected and centrifuged at 2,000 × g for 10 min to remove cellular debris before tangential-flow concentration. The concentrated sample was subsequently centrifuged at 2,000 × g for 30 min and 10,000 × g for 45 min at 4 °C to remove residual cells, debris, and larger vesicles. The supernatant was passed through a 0.45-μm filter and ultracentrifuged at 100,000 × g for 70 min at 4 °C. The pellet was resuspended in 10 mL of cold PBS and subjected to a second ultracentrifugation at 100,000 × g for 70 min at 4 °C. The resulting BMSC-derived exosome preparation was resuspended in PBS and stored at −80 °C until use.

For surface modification of the final functional batch, 1.3 mg of the exosome preparation was mixed with 1.3 mg of FITC-DSPE-PEG2K-cRGDfc. The mixture was incubated at 50 °C for 30 min and then rotated overnight at 4 °C. The reaction mixture was diluted with 10 mL PBS and ultracentrifuged at 100,000 × g for 30 min at 4 °C to remove unbound material. The cRGD-modified exosome pellet was resuspended in 500 μL PBS.

For siRNA loading, the cRGD-modified exosome suspension was concentrated to 240 μL and divided into two 120-μL aliquots. Each aliquot was mixed with 20 μL solution containing 200 pmol of either FOSB siRNA or negative-control siRNA and 10 μL Exo-Fect solution (Exo-Fect Exosome Transfection Kit, SBI, EXFT10A-1). The mixtures were gently inverted three times without vortexing, incubated at 37 °C for 10 min, and immediately placed on ice. EXO Quick-TC reagent was then added to terminate the loading reaction. After six gentle inversions, the preparations were incubated on ice for 30 min and centrifuged at 13,000–14,000 rpm for 3 min. The supernatant was removed, and each pellet was resuspended in 200 μL PBS to obtain cRGD-Exo/si-FOSB or cRGD-Exo/si-NC.

For transmission electron microscopy (TEM), 10 μL of each preparation was deposited onto a copper grid for 1 min, negatively stained with 10 μL uranyl acetate for 1 min, air-dried, and imaged at an accelerating voltage of 80 kV using a Hitachi HT-7700 microscope. Particle size and concentration were measured using a NanoFCM N30E nano-flow cytometer after instrument calibration with the corresponding size and concentration standards. Events within the 30–150 nm size gate were used for descriptive batch characterization. Total protein concentrations were measured using a bicinchoninic acid assay. Exosomal marker proteins CD63 and TSG101 and the non-exosomal/endoplasmic-reticulum marker Calnexin were examined by western blotting, using 293-cell lysate as a positive control and 50 μg protein per lane.

The FITC-positive particle fraction of the final cRGD-modified batch was determined by

nano-flow cytometry using an unlabeled exosome preparation as the blank control. This measurement was used to verify the presence of FITC-associated particles after the surface-modification and purification procedure; it was not interpreted as exosome purity or as a quantitative measure of siRNA encapsulation efficiency.

2.14 PKH26 labeling and cellular uptake of exosome preparations

Exosome preparations were labeled with PKH26 under light-protected conditions. Briefly, 1 μL PKH26 was diluted with 9 μL Diluent C and mixed with the exosome preparation for 10 min at room temperature. The suspension was diluted with 1 mL PBS and ultracentrifuged at 100,000 × g for 17 min. The supernatant was discarded, and the pellet was washed three times with sterile PBS to reduce unbound dye. The final pellet was resuspended in 100 μL sterile PBS. PBS processed using the same labeling procedure served as the dye control.

Podocytes grown on coverslips were incubated with PKH26-labeled exosome preparations at an exosomal protein concentration of 15 μg/mL for 24 h. The cells were then washed three times with PBS, fixed with 4% paraformaldehyde for 30 min at room temperature, counterstained with DAPI for 10 min, and imaged using a Leica SP8 laser-scanning confocal microscope equipped with a 63×/1.40 oil-immersion objective.

2.15 Flow Cytometry Detection of Integrin αvβ3

Normal podocytes and HBx-stably transfected podocytes were divided into six groups: Con group, HBx group, Con+Exo group, Con+cRGD-Exo group, HBx+Exo group, and HBx+cRGD-Exo group. Cells were digested with trypsin, washed twice with pre-cooled PBS, and adjusted to a density of 1×10^6 cells per 100 μL. Cell suspensions were stained with FITC-conjugated anti-human CD51/CD61 antibody at room temperature in the dark for 30 min. After PBS washing and resuspension, samples were analyzed on an Agilent NovoCyte flow cytometer, with 15,000 events acquired per sample to quantify the fluorescence intensity of integrin αvβ3.

2.16 Statistical Analysis

Quantification of Western blot and immunohistochemistry results was performed using ImageJ software. All measurement data were tested for normality and expressed as mean ± standard deviation. Statistical analyses were conducted with GraphPad Prism 10.6.1, with three independent biological replicates set for each group. Two-group comparisons were performed using independent samples t-test, while multiple-group comparisons were analyzed by one-way analysis of variance (ANOVA) followed by Tukey's post-hoc test. $P < 0.05$ was defined as statistically significant.

Results

1. Transcriptome Sequencing Identifies FOSB as a Key Pathogenic Gene in HBV-GN

RNA sequencing was performed on renal biopsy specimens from 3 patients with HBV-GN and 3 healthy controls. Using the thresholds of $|\log_2FC| > 1$ and $q < 0.05$, a total of 570 differentially expressed genes (DEGs) were screened, including 200 upregulated genes (35.1%) and 370 downregulated genes (64.9%) (Figure 1A). Gene Ontology (GO) enrichment analysis revealed that these DEGs were mainly enriched in biological processes such as regulation of immune response, defense response, regulation of cell adhesion and leukocyte activation (Figure 1B). Kyoto Encyclopedia of Genes and Genomes (KEGG) pathway analysis further demonstrated significant enrichment of immune-inflammatory pathways, including the T cell receptor signaling pathway, chemokine signaling pathway, Th17 cell differentiation, cell adhesion molecules,

cytokine-cytokine receptor interaction and IL-17 signaling pathway (Figure 1C). Notably, among the 8 DEGs enriched in the IL-17 signaling pathway, only FOSB was markedly upregulated, whereas the other seven genes (MMP9, TNFAIP3, CXCL6, LCN2, CXCL1, IKBKE, IKBKG) were all downregulated (Figure 1D).

The IL-17 signaling pathway modulates the transcription of downstream inflammatory genes by activating the AP-1 transcription complex. As a subunit of AP-1, FOSB forms heterodimers with JUN proteins to regulate the transcription of pro-inflammatory genes including MMPs, chemokines and cytokines. Previous studies have reported aberrant FOSB expression in multiple renal diseases such as acute kidney injury (AKI), diabetic kidney disease (DKD) and IgA nephropathy, which is closely correlated with disease progression. Combining the above transcriptomic screening results and published literature, FOSB was selected as the core candidate target for subsequent investigations.

Figure 1 Transcriptome sequencing analysis of renal tissues from HBV-GN patients.

(A) Volcano plot of differentially expressed genes (DEGs) between renal tissues of HBV-GN patients and healthy controls. (B) Gene Ontology biological process (GO-BP) enrichment analysis. (C) KEGG pathway enrichment analysis of DEGs. (D) Heatmap exhibiting gene expression profiles in the IL-17 signaling pathway.

2.FOSB silencing reverses HBx-induced podocyte injury

HBx-stimulated human podocytes (HPCs) were transfected with FOSB siRNA or negative control (NC) siRNA, respectively. Compared with the Con group, the mRNA and protein levels of FOSB were markedly elevated in HBx-treated HPCs (Figure 2A~B), verifying that HBx triggers aberrant FOSB expression at both transcriptional and translational levels. Immunofluorescence staining revealed that the fluorescence intensity of podocyte-specific marker Nephrin was significantly decreased, while the injury marker Desmin was drastically increased in HBx-exposed podocytes, demonstrating that HBx-mediated FOSB overexpression leads to podocyte damage (Figure 2C). After transfection with FOSB siRNA to knock down FOSB, the mRNA and protein abundance of FOSB were remarkably reduced relative to HBx podocytes treated with NC siRNA, accompanied by obvious alleviation of podocyte injury phenotypes.

Figure 2 HBx induces FOSB overexpression and dysregulation of podocyte markers, and FOSB silencing restores normal podocyte phenotype.

(A~B) Relative FOSB mRNA and protein expression in podocytes of each group detected by RT-qPCR and Western blot, with GAPDH as the internal reference (n=3). (C) Immunofluorescence staining for FOSB, Nephrin and Desmin in podocytes; nuclei were stained with DAPI, representative images (scale bar: 50 μm). Data are presented as mean ± SD. ***$p < 0.001$, **$p < 0.01$ vs. Con group; ns, no significant difference compared with the HBx+si-NC group.

3.FOSB silencing reverses HBx-induced abnormal invasion, apoptosis and inflammatory response in podocytes

To systematically evaluate the essential function of FOSB in HBx-triggered podocyte injury, we performed siRNA-mediated FOSB knockdown and simultaneously detected podocyte invasive capacity, proliferative activity, apoptotic level and pro-inflammatory cytokine expression, so as to clarify whether FOSB acts as a key downstream effector of HBx to orchestrate the above pathological processes. Transwell assays revealed that HBx overexpression markedly elevated podocyte invasion compared with the control group, whereas FOSB silencing effectively reversed

this phenotype, indicating that FOSB participates in HBx-mediated structural disruption of the glomerular filtration barrier (Figure 3A). CCK-8 assays further demonstrated that HBx significantly facilitated podocyte proliferation, and this proliferative activity was remarkably suppressed after FOSB knockdown, suggesting that FOSB-driven aberrant proliferation may serve as the cellular basis for enhanced podocyte invasion (Figure 3B). Flow cytometry with Annexin V/PI double staining showed that HBx robustly induced podocyte apoptosis, while the apoptosis rate was greatly reduced upon FOSB silencing, implying that enhanced invasion and apoptotic imbalance share a FOSB-dependent regulatory pathway (Figure 3C). Western blot results further verified elevated caspase-3 expression in the HBx group, which was significantly downregulated after FOSB knockdown. Meanwhile, the level of phosphorylated histone H3 (p-H3) was decreased in HBx-treated podocytes and restored following FOSB silencing, revealing that FOSB may modulate podocyte survival by regulating cell cycle-related signaling (Figure 3D). In addition, ELISA assays demonstrated that HBx stimulation promoted the secretion of pro-inflammatory cytokines including IL-1β, IL-18 and TNF-α in podocytes, and FOSB knockdown markedly suppressed the release of all these cytokines. Collectively, these data indicate that FOSB functions as a central downstream hub of HBx to cooperatively drive the cascade of podocyte invasion, proliferation, apoptosis and inflammation, forming an amplifying network of podocyte injury in HBV-GN (Figure 3E).

Figure 3 FOSB silencing reverses HBx-induced abnormal invasion, proliferation, apoptosis and inflammatory response in podocytes.

(A) Transwell assay for podocyte invasive capacity, representative images (scale bar: 50 μm) and quantitative statistics (n=3); (B) CCK-8 assay for podocyte proliferative activity at different time points (n=3); (C) Flow cytometry with Annexin V/PI double staining to detect apoptotic rate, representative dot plots and quantitative analysis (n = 3); (D) Western blot analysis of caspase-3 and p-H3 protein levels, with β-actin and total H3 as internal references, respectively (n=3);(E) ELISA measurement of IL-1β, IL-18 and TNF-α concentrations in cell culture supernatants (n=3). Data are presented as mean ± SD. *$p < 0.05$, **$p < 0.01$, ***$p < 0.001$ vs. Con group; ns, no significant difference compared with the HBx+si-NC group.

4. AAV-mediated kidney-specific FOSB knockdown ameliorates renal dysfunction and pathological lesions in HBx transgenic mice

To further verify the in vivo protective effect of FOSB silencing, tail vein injection of AAV-shFOSB was applied to achieve kidney-specific FOSB knockdown in HBx transgenic mice. We systematically evaluated its therapeutic effects on HBx-triggered renal pathological injury, abnormal renal function, expression of podocyte markers, cellular apoptosis and inflammatory response.RT-qPCR and Western blot analyses confirmed that the mRNA and protein levels of FOSB were significantly elevated in renal tissues of HBx transgenic mice relative to control mice, while AAV-shFOSB intervention efficiently downregulated FOSB expression, indicating successful renal FOSB silencing mediated by the AAV vector (Figure 4A~B). Immunofluorescence staining revealed attenuated Nephrin expression, enhanced Desmin expression and disordered distribution of podocyte markers in the HBx group. After AAV-shFOSB administration, Nephrin expression was restored and Desmin abundance was reduced, leading to effective protection of podocyte phenotype (Figure 4C).HE staining exhibited obvious glomerular structural disorder, widened mesangial area and vacuolar degeneration of renal tubular epithelial cells in HBx transgenic mice, whereas these pathological alterations were markedly alleviated

upon AAV-shFOSB treatment (Figure 5A). Renal function assays demonstrated that serum creatinine (SCr), blood urea nitrogen (BUN) and 24-hour urinary total protein (24h-UTP) were drastically increased in the HBx group compared with controls, and all indicators were prominently decreased after AAV-shFOSB intervention, suggesting that FOSB silencing effectively rescues HBx-induced renal dysfunction (Figure 5A).Western blot detection of apoptosis-related proteins in renal tissues showed upregulated caspase-3 in the HBx group, which was significantly reduced by AAV-shFOSB treatment. Meanwhile, the level of phosphorylated histone H3 (p-H3) was suppressed in HBx mice and recovered after FOSB knockdown. These findings were consistent with in vitro cellular data, demonstrating that FOSB participates in podocyte injury by modulating apoptotic and cell cycle signaling both in vitro and in vivo (Figure 5B).Immunohistochemical staining further revealed massive infiltration of F4/80-positive macrophages in renal tissues of the HBx group, and the positive staining area was markedly reduced after AAV-shFOSB administration, indicating that FOSB silencing suppresses local renal inflammatory cell recruitment (Figure 5C). ELISA measurement of serum inflammatory cytokines showed significantly higher concentrations of IL-1β, IL-18 and TNF-α in the HBx group than controls, and the secretion of all three cytokines was remarkably inhibited by AAV-shFOSB (**$p < 0.01$, ***$p < 0.001$). These results suggest that FOSB acts as a critical downstream regulator of HBx to synergistically drive the renal apoptosis-inflammation cascade in vivo (Figure 5D–E).
Collectively, the in vivo experimental results corroborate the in vitro cellular findings, jointly supporting that FOSB serves as a core effector target responsible for podocyte injury in HBV-GN.
Figure 4 AAV-mediated kidney-specific FOSB silencing restores the expression of podocyte markers in HBx transgenic mice.
(A) RT-qPCR analysis of FOSB mRNA levels in renal tissues of mice from each group (n=3); (B) Western blot detection of FOSB protein in mouse renal tissues, with GAPDH as the internal reference (n = 3); (C) Immunofluorescence staining for the expression and localization of FOSB, Nephrin and Desmin in renal tissues; nuclei were counterstained with DAPI, representative images (scale bar:20 μm). Data are presented as mean ± SD. ***$p < 0.001$ vs. Con group; ns, no significant difference compared with the HBx+AAV-shNC group.
Figure 5 AAV-mediated kidney-specific FOSB silencing alleviates renal pathological lesions, renal dysfunction and inflammatory response in HBx transgenic mice.
(A) Representative HE staining images showing renal pathological changes (scale bar:20 μm) .(B) detection of renal function indicators (SCr, BUN, 24h-UTP) (n=3); (C) Western blot analysis of caspase-3 and p-H3 protein expression in renal tissues (n=3); (D) Immunohistochemical staining for F4/80-positive macrophage infiltration in kidneys, representative images (scale bar:50 μm) and quantitative analysis of positive staining area (n=3); (E) ELISA detection of serum IL-1β, IL-18 and TNF-α concentrations (n=3). Data are presented as mean ± SD. *$p < 0.05$, **$p < 0.01$, ***$p < 0.001$ vs. Con group; ns, no significant difference compared with the HBx+AAV-shNC group.
5. Preparation and batch characterization of cRGD-modified BMSC-derived exosomes loaded with FOSB siRNA

BMSC-derived exosomes were isolated by sequential centrifugation, tangential-flow concentration, and ultracentrifugation. Western blotting detected the exosomal markers CD63 and TSG101 in the isolated preparation, whereas Calnexin was not detected in the exosome lane; the corresponding positive-control signal was retained in the source blot (Figure 6A). Together with the vesicular morphology observed by TEM, these findings were consistent with an

exosome-enriched extracellular-vesicle preparation.

Nano-flow cytometry provided complete particle-size and concentration profiles for the four formulations used during the engineering procedure (Figure 6B and Table 2). Native Exo had a mean diameter of 80.0 nm (median, 76.2 nm; SD, 16.1 nm), with 98.74% of detected events within the 30–150 nm gate and a particle concentration of 4.90×10^{10} particles/mL. After cRGD modification, cRGD-Exo had a mean diameter of 86.3 nm (median, 81.8 nm; SD, 19.0 nm), a gated fraction of 97.65%, and a particle concentration of 2.48×10^{10} particles/mL. Following the siRNA-loading and purification procedure, cRGD-Exo/si-NC and cRGD-Exo/si-FOSB had mean diameters of 88.9 and 89.7 nm, respectively. Their corresponding median diameters were 84.8 and 85.8 nm, SD values were 17.9 and 19.0 nm, gated fractions were 84.51% and 83.99%, and particle concentrations were 4.73×10^{9} and 4.96×10^{9} particles/mL, respectively. Thus, all four preparations retained mean particle diameters below 100 nm, although particle recovery was lower after the siRNA-loading and purification procedure. These measurements represent descriptive characterization of the functional preparation batch and were not subjected to inferential statistical testing.

Nano-flow cytometry of the final peptide-modified preparation showed that 32.6% of analyzed particles were FITC-positive under the predefined gate (1,419 of 4,355 events), whereas the unlabeled blank control contained no FITC-positive events (0 of 2,658 events) (Figure 6C). This result verified a FITC-positive particle population after cRGD modification and removal of unbound material. The percentage was not used as a measure of exosome purity, coupling efficiency, or siRNA encapsulation efficiency.

TEM images acquired at multiple magnifications showed membrane-bound, cup-shaped particles in the native Exo, cRGD-Exo, cRGD-Exo/si-NC, and cRGD-Exo/si-FOSB preparations (Figure 6D and Supplementary Figure S1). No marked morphological disruption was apparent after cRGD modification or Exo-Fect-mediated siRNA loading. The corresponding BCA protein concentrations were 1.018215 μg/μL for native Exo, 0.5564965 μg/μL for cRGD-Exo/si-NC, and 0.572411 μg/μL for cRGD-Exo/si-FOSB (Supplementary Table S1).

Confocal microscopy showed that in the PBS control group, only DAPI-stained nuclei (blue) were visible, with no detectable PKH26 fluorescence (red), confirming a clean red fluorescence background and the absence of exosome uptake. In the unmodified exosome (Exo) group, red fluorescence was observed in the cytoplasm of podocytes, indicating cellular internalization of the exosomes. In the cRGD-Exo group, the red fluorescence signal appeared more pronounced and more widely distributed in the cytoplasm than in the Exo group; however, because the available experiment did not include receptor blocking or a validated quantitative uptake comparison across independent biological replicates, this observation alone did not establish enhanced cRGD-dependent uptake. Consistent internalization was observed across the representative fields. Bright-field (BF) images showed that cells in all groups maintained good morphology and normal adherence, excluding the possibility that the fluorescence signals originated from cellular debris or background (Figure 6E and Supplementary Figure S2).

Figure 6. Characterization of cRGD-FITC-modified exosomes and cellular uptake.

(A)Western blot analysis of the exosomal markers CD63 and TSG101 and the non-exosomal/endoplasmic-reticulum marker Calnexin in the isolated exosome preparation; 293-cell lysate was used as a positive control. Uncropped blots are provided in the Source Data. (B) Nano-flow cytometry particle-size distributions of native BMSC-derived exosomes (Exo),

cRGD-modified exosomes (cRGD-Exo), cRGD-modified exosomes loaded with negative-control siRNA (cRGD-Exo/si-NC), and cRGD-modified exosomes loaded with FOSB siRNA (cRGD-Exo/si-FOSB). A descriptive summary of the mean diameter, median diameter, standard deviation, fraction of particles within the 30–150 nm gate, and particle concentration for each preparation is provided in Table 2. The measurements represent batch characterization outputs; no inferential statistical comparisons were performed.(C) Nano-flow cytometry analysis of FITC-positive particles in the final cRGD-modified exosome preparation and the unlabeled blank control. The FITC-positive fractions were 32.6% (1,419/4,355 events) and 0.0% (0/2,658 events), respectively. Left: cRGD-FITC-modified exosomes; Right: blank control.(D) Representative TEM images of Exo, cRGD-Exo, cRGD-Exo/si-NC, and cRGD-Exo/si-FOSB. Scale bars, 100 nm. Additional fields and magnifications are provided in Supplementary Figure S1. (E) Representative confocal images of podocytes incubated with PKH26-labeled native or peptide-modified exosome preparations; PBS processed using the same dye-labeling procedure served as the control. BF, bright field; DAPI, nuclear staining; PKH26, exosome label. Scale bar, 100 μm.Additional fields and individual channels are provided in Supplementary Figure S2.

Table2 Nano-flow cytometry characterization of exosome preparations used in the engineering workflow.

Preparation	Median diameter (nm)	Mean diameter (nm)	SD (nm)	Events within 30–150 nm gate (%)	Particle concentration (particles/mL)
Exo	76.2	80.0	16.1	98.74	4.90×10^{10}
cRGD-Exo	81.8	86.3	19.0	97.65	2.48×10^{10}
cRGD-Exo/si-NC	84.8	88.9	17.9	84.51	4.73×10^{9}
cRGD-Exo/si-FOSB	85.8	89.7	19.0	83.99	4.96×10^{9}

6.cRGD-modified exosomes restore HBx-induced upregulation of integrin αvβ3 in podocytes

Flow cytometry was used to assess integrin αvβ3 expression in podocytes in each group (Figure 7A), and the fluorescence intensity was quantified (Figure 7B). Histograms showed that integrin αvβ3 fluorescence intensity was comparable among the control, control + Exo, and control + cRGD-Exo groups, indicating that exosome treatment did not affect basal αvβ3 expression in normal podocytes. In contrast, αvβ3 expression was significantly upregulated in the hepatitis B virus X protein (HBx) group. In the HBx-injury model, treatment with native exosomes (Exo) had only a marginal effect on αvβ3 levels, whereas treatment with arginine-glycine-aspartic acid cyclic peptide (cRGD)-modified exosomes (cRGD-Exo) significantly restored αvβ3 expression. Quantitative analysis confirmed that HBx-induced podocyte injury led to abnormal upregulation of integrin αvβ3, which was reversed by cRGD-Exo treatment; meanwhile, exosome treatment, regardless of cRGD modification, had no significant

effect on αvβ3 expression in normal podocytes.

Figure 7. Flow cytometric analysis of integrin αvβ3 expression in podocytes. (A) Representative flow cytometry histograms showing integrin αvβ3 expression in podocytes from each group. (B) Quantitative analysis of αvβ3 fluorescence intensity. Podocytes were untreated (Con) or treated with HBx, and were subsequently left untreated or treated with native exosomes (Exo) or cRGD-modified exosomes (cRGD-Exo) as indicated (Con+Exo, Con+cRGD+Exo, HBX+Exo, HBX+cRGD+Exo). Data are expressed as mean ± standard deviation (SD) from n = 3 independent experiments. $p < 0.05$, $^{**}p < 0.001$; ns, no significant difference.

7.cRGD-modified exosomes carrying FOSB siRNA alleviate HBx-induced podocyte injury via specific FOSB silencing

After successfully constructing the cRGD-modified targeted exosome vector, we further verified its therapeutic efficacy against HBx-induced podocyte injury following loading with FOSB siRNA. HBx-stably transfected podocytes were randomly divided into four groups: PBS control group, native exosome group (Exo), cRGD-Exo loaded with si-NC group (cRGD-Exo/si-NC), and cRGD-Exo loaded with si-FOSB group (cRGD-Exo/si-FOSB). RT-qPCR and Western blot analyses revealed that, compared with the PBS group, there was no significant change in FOSB expression in the native Exo and cRGD-Exo/si-NC groups, whereas FOSB mRNA and protein levels were markedly downregulated in the cRGD-Exo/si-FOSB group, confirming that targeted exosomes successfully mediated FOSB silencing in podocytes (Figure8A~B). Immunofluorescence staining further demonstrated that the PBS and native Exo groups exhibited high FOSB expression, reduced Nephrin expression and increased Desmin expression; the cRGD-Exo/si-NC group showed a similar phenotype to the PBS group. In contrast, the cRGD-Exo/si-FOSB group displayed significantly weakened FOSB fluorescence signals, restored Nephrin expression and decreased Desmin expression, indicating effective correction of the disordered podocyte marker phenotype (Figure8C). Collectively, these results demonstrate that cRGD-modified exosomes carrying FOSB siRNA can efficiently deliver the siRNA to HBx-induced injured podocytes and restore the normal podocyte phenotype through specific FOSB silencing, providing in vitro functional evidence for the targeted therapy of HBV-GN using engineered exosomes.

Figure8 cRGD-modified exosomes loaded with FOSB siRNA silence FOSB and rescue the abnormal phenotype of HBx-induced injured podocytes. (A) RT-qPCR assay was performed to determine FOSB mRNA expression levels in podocytes of each group (n = 3); (B) Western blot analysis was used to detect FOSB protein expression in podocytes of each group, with GAPDH serving as the internal reference (n = 3); (C) Immunofluorescence staining was conducted to evaluate the expression and subcellular localization of FOSB, Nephrin and Desmin in podocytes of each group; nuclei were counterstained with DAPI, and representative images are shown (scale bar: 50 μm). Data are expressed as mean ± standard deviation (SD). $^{***}p < 0.001$ compared with the HBx+PBS group; ns indicates no significant difference.

7.cRGD-modified exosomes carrying FOSB siRNA reverse HBx-induced podocyte functional abnormalities and inflammatory activation

Having confirmed that cRGD-Exo/si-FOSB could effectively restore FOSB expression and normalize podocyte marker phenotype in HBx-induced podocytes, we further systematically evaluated the intervention effects of this engineered exosome on podocyte functional phenotypes. Transwell assay results showed that, compared with the PBS group, the invasive capacity of

HBx-stably transfected podocytes was significantly enhanced; treatment with native Exo or cRGD-Exo/si-NC had no significant effect on invasive capacity, whereas the number of invasive cells was drastically reduced after cRGD-Exo/si-FOSB treatment, suggesting that FOSB siRNA delivered by targeted exosomes could effectively reverse HBx-mediated abnormal podocyte invasion (Figure 9A). CCK-8 assays demonstrated that native Exo and cRGD-Exo/si-NC had no obvious impact on HBx-induced podocyte proliferative activity, while cRGD-Exo/si-FOSB significantly suppressed aberrant proliferation, indicating that FOSB silencing could restore the normal proliferation homeostasis of podocytes (Figure 9B). Flow cytometry with Annexin V/PI double staining revealed that the apoptotic rate was significantly increased in the HBx+PBS group, with no obvious changes in the native Exo and cRGD-Exo/si-NC groups; cRGD-Exo/si-FOSB treatment markedly decreased the apoptotic rate, suggesting that targeted exosomes effectively alleviate HBx-induced podocyte apoptosis by silencing FOSB (Figure 9C). Western blot analysis further verified that the expression of caspase-3 was significantly lower in the cRGD-Exo/si-FOSB group than in the control group, while p-H3 expression was remarkably restored, which was consistent with the results of direct siRNA transfection in vitro, indicating that the engineered exosome delivery system could successfully recapitulate the biological effects of FOSB silencing (Figure 9D). In addition, ELISA assays showed that the secretion of IL-1β, IL-18 and TNF-α was significantly inhibited after cRGD-Exo/si-FOSB treatment, whereas native Exo and cRGD-Exo/si-NC had no significant effect on inflammatory cytokine levels, confirming that targeted exosomes could specifically deliver FOSB siRNA to effectively block the HBx-induced inflammatory cascade in podocytes (Figure 9E). Collectively, these results demonstrate that cRGD-modified exosomes carrying FOSB siRNA can precisely deliver the siRNA and synergistically reverse HBx-mediated podocyte invasion, proliferation, apoptosis and inflammatory cascade responses in vitro, providing reliable functional evidence for cell-free targeted therapy of HBV-GN.

Figure9 cRGD-Exo/si-FOSB reverses HBx-induced abnormal podocyte invasion, proliferation, apoptosis and inflammatory response. (A) Transwell assay for evaluating podocyte invasive capacity in each group, with representative images (scale bar: 50 μm) and quantitative statistics (n = 3); (B) CCK-8 assay for detecting podocyte proliferative activity in each group (n= 3); (C) Flow cytometry with Annexin V/PI double staining for measuring cell apoptotic rate, showing representative dot plots and quantitative statistics (n=3); (D) Western blot analysis of caspase-3 and p-H3 protein expression, with β-actin and total H3 serving as internal references, respectively (n=3); (E) ELISA measurement of IL-1β, IL-18 and TNF-α concentrations in cell culture supernatants (n=3). Data are expressed as mean ± standard deviation (SD). **$p < 0.01$, ***$p < 0.001$ compared with the HBx+PBS group; ns indicates no significant difference.

8.cRGD-modified exosomes carrying FOSB siRNA alleviate HBx-induced renal injury in HBx transgenic mice

After verifying that cRGD-Exo/si-FOSB could effectively reverse HBx-induced podocyte injury phenotypes in vitro, we further evaluated the in vivo therapeutic efficacy of this engineered exosome in HBx transgenic mice. Mice were randomly divided into five groups: normal control group (Con), HBx transgenic group (HBx), HBx+native Exo group, HBx+cRGD-Exo/si-NC group, and HBx+cRGD-Exo/si-FOSB group, with administration via tail vein injection. RT-qPCR and Western blot analyses showed that FOSB mRNA and protein levels in renal tissues of the HBx group were significantly higher than those in the Con group; treatment with native Exo or

cRGD-Exo/si-NC had no significant effect on FOSB expression, whereas FOSB expression was markedly downregulated in the HBx+cRGD-Exo/si-FOSB group, confirming that targeted exosomes successfully mediated renal FOSB silencing in vivo (Figure10A–B). Immunofluorescence staining revealed high FOSB expression, reduced Nephrin expression and increased Desmin expression in glomeruli of the HBx group; after cRGD-Exo/si-FOSB treatment, FOSB fluorescence signals were significantly weakened, Nephrin expression was restored and Desmin expression was decreased, indicating effective correction of the disordered podocyte marker phenotype (Figure 10C). HE staining demonstrated obvious glomerular structural disorder, widened mesangial area and vacuolar degeneration of renal tubular epithelial cells in the HBx group; pathological changes in the native Exo and cRGD-Exo/si-NC groups were similar to those in the HBx group, while the above lesions were significantly alleviated in the cRGD-Exo/si-FOSB group (Figure11A). Renal function assays indicated that serum creatinine (SCr), blood urea nitrogen (BUN) and 24-hour urinary total protein (24h-UTP) levels in the HBx group were significantly elevated compared with the Con group; native Exo and cRGD-Exo/si-NC had no significant improvement effect on these indicators, whereas SCr, BUN and 24h-UTP levels were drastically reduced after cRGD-Exo/si-FOSB intervention, suggesting that targeted exosomes could effectively ameliorate HBx-induced renal dysfunction (Figure11B). Western blot analysis showed that caspase-3 expression in renal tissues of the cRGD-Exo/si-FOSB group was significantly lower than that in the HBx group, while p-H3 expression was remarkably restored, which was consistent with the results of AAV-shFOSB intervention and in vitro cellular experiments, indicating that the engineered exosome delivery system also exerted anti-apoptotic effects via FOSB silencing in vivo (Figure11C). Immunohistochemical staining revealed a significant increase in F4/80-positive macrophage infiltration in renal tissues of the HBx group; no obvious improvement was observed in the native Exo and cRGD-Exo/si-NC groups, while the positive staining area was drastically reduced after cRGD-Exo/si-FOSB treatment, suggesting that targeted exosomes could inhibit local renal inflammatory cell recruitment (Figure11D). ELISA measurement of serum inflammatory cytokines confirmed that IL-1β, IL-18 and TNF-α concentrations in the HBx group were significantly higher than those in the Con group; cRGD-Exo/si-FOSB intervention markedly inhibited the secretion of all these cytokines, whereas native Exo and cRGD-Exo/si-NC had no significant effect on inflammatory cytokine levels (Figure 11E).Collectively, these in vivo findings demonstrate that cRGD-modified exosomes carrying FOSB siRNA precisely deliver the siRNA to injured renal tissue and reverse HBx-triggered renal pathological damage, renal dysfunction, apoptosis and inflammatory response, offering comprehensive in vivo functional validation for engineered exosome-targeted therapy of HBV-GN.

Figure10 cRGD-modified exosomes carrying FOSB siRNA mediate renal FOSB silencing and restore podocyte marker expression in HBx transgenic mice. (A) RT-qPCR analysis of FOSB mRNA expression levels in renal tissues of mice from each group (n=3); (B) Western blot detection of FOSB protein expression in renal tissues of mice from each group, with GAPDH as the internal reference (n=3); (C) Immunofluorescence staining for the expression and localization of FOSB, Nephrin and Desmin in renal tissues; nuclei were counterstained with DAPI, representative images (scale bar: 20 μm). Data are expressed as mean ± standard deviation (SD). $^{**}p < 0.01$, $^{***}p < 0.001$ vs. Con group; $^{**}p < 0.01$ vs. HBx group; ns indicates no significant difference.

Figure 11 cRGD-modified exosomes carrying FOSB siRNA ameliorate renal pathological damage, renal dysfunction and inflammatory response in HBx transgenic mice.(A) HE staining for observing renal pathological changes in mice from each group (scale bar: 50 μm); (B) Biochemical detection of SCr, BUN and 24h-UTP levels in mice from each group (n=3); (C) Western blot analysis of caspase-3 and p-H3/total H3 protein expression in renal tissues (n=3); (D) Immunohistochemical staining for F4/80-positive macrophage infiltration in renal tissues, showing representative images (scale bar: 50 μm) and quantitative statistical analysis of positive staining area (n=3); (E) ELISA measurement of IL-1β, IL-18 and TNF-α concentrations in serum (n=3). Data are expressed as mean ± standard deviation (SD). *$p < 0.05$, **$p < 0.01$, ***$p < 0.001$ vs. Con group; ns indicates no significant difference compared with the HBx group.

Discussion

Hepatitis B virus (HBV) infection poses a critical public health crisis worldwide[22]. The virus exhibits broad tissue tropism and can induce a spectrum of extrahepatic lesions apart from hepatic injury, among which hepatitis B virus-associated glomerulonephritis (HBV-GN) is the most prevalent subtype[23]. Glomerular podocytes constitute the core component of the glomerular filtration barrier and serve as the primary target of pathological damage in HBV-GN[24]. Persistent stimulation triggers podocyte foot process fusion, detachment and apoptosis, ultimately leading to persistent proteinuria and progressive glomerulosclerosis[25, 26]. As a 17 kDa multifunctional regulatory protein consisting of 154 amino acids encoded by HBV, HBx modulates multiple intracellular signaling cascades to govern cell cycle progression, apoptosis and inflammatory responses, acting as a central pathogenic mediator of HBV-induced hepatic and renal injuries[27, 28].

FBJ murine osteosarcoma viral oncogene homolog B (FOSB) belongs to the Fos transcription factor family, which heterodimerizes with JUN to form the AP-1 complex and drives the transcription of numerous target genes associated with proliferation and inflammation[29-31]. Existing literature has linked FOSB to multiple systemic disorders: in the central nervous system, FOSB is regarded as a potential therapeutic target for depression; within nephrology, elevated FOSB expression correlates with disease severity in patients with IgA nephropathy, and upregulated FOSB is detected in thalamic nuclei in renal ischemia-reperfusion animal models[32-34]. Additionally, microRNA-27A-3P modulates podocyte function in IgA nephritis via targeting FOSB[35]. Despite these observations, the specific pathogenic role of FOSB in HBV-GN remains uncharacterized. In the present study, transcriptome sequencing was performed on renal biopsy specimens from HBV-GN patients and healthy controls. Bioinformatic enrichment analyses revealed prominent enrichment of the IL-17 signaling pathway in diseased renal tissues, with FOSB identified as the sole significantly upregulated differential gene within this cascade. Subsequent in vitro podocyte experiments and in vivo HBx transgenic mouse models consistently demonstrated that HBx stimulation elevates FOSB expression concurrent with podocyte injury. Silencing FOSB via in vitro siRNA transfection or kidney-specific AAV-shFOSB injection markedly alleviated HBx-triggered podocyte lesions. Collectively, these data verify that FOSB functions as a vital downstream effector of HBx that drives podocyte damage, occupying a pivotal position in the initiation and progression of HBV-GN. This study integrates FOSB into the HBx pathogenic regulatory network and offers a novel theoretical framework to elucidate the molecular mechanisms underlying HBx-mediated podocyte injury.

Dysregulated apoptosis homeostasis governs physiological stability and pathological progression across numerous disorders, including malignancies, autoimmune diseases and neurodegenerative diseases[36, 37]. Three primary apoptotic cascades have been identified: the extrinsic death receptor pathway, intrinsic mitochondrial pathway and endoplasmic reticulum stress-mediated pathway[38, 39]. Prior studies have validated that HBx directly targets mitochondria, opening the mitochondrial permeability transition pore, depolarizing mitochondrial membrane potential, and facilitating the cytoplasmic release of cytochrome c and apoptosis-inducing factor to activate the caspase cascade sequentially[40, 41]. Flow cytometry and western blot analyses in this study illustrated elevated expression of the apoptosis executioner caspase-3 and increased apoptotic rates in HBx-overexpressing podocytes, whereas FOSB inhibition robustly reversed these phenotypes; identical results were recapitulated in HBx transgenic mice, indicating that

FOSB is an indispensable intermediate mediator linking HBx to mitochondrial apoptosis in podocytes.

Cell invasion, a specialized form of cell migration that enables cells to degrade and traverse basement membranes and extracellular matrices, participates in wound healing, angiogenesis, inflammatory infiltration and tumor metastasis[42, 43]. Transwell invasion assays demonstrated that HBx drastically enhances podocyte invasive capacity, while FOSB silencing completely rescues this aberrant phenotype, suggesting that FOSB-dependent transcriptional programs underpin HBx-mediated disruption of the glomerular filtration barrier.

Macrophage activation and infiltration amplify chronic glomerular injury continuously[44]. The recently proposed podocyte-macrophage transition (PMT) paradigm further advances our understanding of renal inflammation, wherein injured podocytes lose intrinsic cellular identity, acquire macrophage-like characteristics, and secrete abundant pro-inflammatory cytokines to sustain local inflammatory bursts[45, 46]. Consistent with previous IgA nephropathy research, our in vivo data exhibited robust F4/80-positive macrophage infiltration alongside elevated circulating and renal levels of IL-1β, IL-18 and TNF-α in HBx transgenic mice, all of which were substantially attenuated following FOSB suppression[47]. Combined with our group’s previous findings that HBx induces podocyte pyroptosis via the NLRP3 inflammasome and ferroptosis through dysregulated iron metabolism, the current work proposes that HBx upregulates FOSB to simultaneously trigger podocyte apoptosis, aberrant invasion and renal inflammatory infiltration, forming a self-amplifying pathological loop.

Nevertheless, this study only confirms the upstream-downstream regulatory relationship between HBx and FOSB. Further multi-omics combined with molecular interaction assays such as dual-luciferase reporter and ChIP tests are required to clarify whether HBx directly binds the FOSB promoter or indirectly modulates FOSB through the IL17-AP-1 axis, as well as to screen the direct downstream target genes of FOSB that mediate apoptosis and inflammation, thereby refining the complete molecular regulatory network of HBV-GN.

Mesenchymal stem cells (MSCs) possess self-renewal capacity and multipotent differentiation potential[48]. Accumulating evidence indicates that the therapeutic benefits of MSCs are predominantly mediated by paracrine secretion of extracellular vesicles rather than direct cell engraftment and differentiation. Exosomes, 30–150 nm lipid bilayer vesicles carrying proteins, lipids, mRNA and microRNAs, mediate intercellular communication[49]. Compared with intact MSCs, MSC-derived exosomes feature low immunogenicity, favorable storage stability and facile surface modification, rendering them a leading candidate for cell-free therapy[50]. However, native exosomes encounter inherent limitations for in vivo RNA interference applications: intravenous administration results in rapid clearance by the mononuclear phagocyte system, leading to minimal accumulation in glomerular podocytes; their short blood circulation half-life renders encapsulated free siRNA susceptible to nuclease degradation, and their limited nucleic acid loading capacity restricts efficient target gene silencing[51, 52]. Consistent with this notion, our data showed that native BMSC-derived exosomes only mildly suppress inflammatory cytokine secretion, fail to downregulate FOSB, and cannot reverse HBx-induced podocyte apoptosis and cytoskeletal disruption, highlighting that endogenous paracrine factors alone are insufficient to block FOSB-dependent injury pathways, necessitating bioengineering modification to optimize carrier performance.

Integrin αvβ3 is highly enriched on the membrane of injured podocytes, and the cyclic

peptide Cyclo(RGDfC) specifically recognizes this receptor to facilitate cellular internalization via receptor-mediated endocytosis, serving as a classic targeting ligand for glomerular delivery[53, 54]. Drawing on existing engineering strategies reported in oncology, cardiovascular and nephrological research, we constructed Cyclo(RGDfC)-modified exosomes loaded with FOSB siRNA derived from BMSCs and validated their therapeutic efficacy in HBV-GN in vitro and in vivo. Serial characterization experiments confirmed that modified exosomes retain intact vesicular morphology with stable expression of canonical exosomal markers CD63 and TSG101, without detectable endoplasmic reticulum contamination marker Calnexin. In vitro functional assays revealed that cRGD-modified exosomes carrying FOSB siRNA effectively silence FOSB, restore physiological podocyte phenotype, and attenuate apoptosis, invasion and inflammatory response. Tail vein delivery in HBx transgenic mice recapitulated these protective effects in vivo: the targeted exosomes downregulated renal FOSB, ameliorated glomerular injury, inhibited renal apoptosis and macrophage infiltration, and restored renal function. Unlike AAV viral vectors, exosomes have no risk of genomic integration and trigger weaker immune responses after repeated administration, rendering them preferable for long-term treatment of chronic renal diseases including HBV-GN.

Several unresolved limitations of this delivery system merit objective discussion. PKH26 fluorescent tracing in vitro illustrated comparable internalization efficiency of native and cRGD-modified exosomes in podocytes, with no obvious uptake enhancement induced by peptide modification. Moreover, constrained by experimental timelines, we did not perform in vivo fluorescence organ tracing to quantify differential exosome biodistribution, lacking direct in vivo evidence that Cyclo(RGDfC) augments renal enrichment. The experimental design also omitted critical control groups including free siRNA and unmodified siRNA-loaded exosomes, which impedes precise discrimination of the independent biological functions of targeting peptide, vesicle carrier and siRNA, and precludes quantitative evaluation of the therapeutic gain conferred by cRGD conjugation. These drawbacks will be prioritized in subsequent investigations. Additionally, the in vitro HBx-stably transfected podocyte line and HBx transgenic mouse model adopted in this study are widely utilized for HBV-associated hepatic disease research, yet they only recapitulate direct HBx cytotoxicity and fail to recapitulate core pathological hallmarks of clinical HBV-GN, including persistent complete HBV infection, circulating immune complex deposition and multi-immune cell crosstalk. Future studies employing clinically relevant animal models and large clinical biopsy cohorts are warranted to validate our conclusions. Despite the promising renoprotective outcomes observed in animal studies, substantial translational barriers remain prior to clinical implementation of engineered exosomes. At the manufacturing level, GMP-compliant large-scale serum-free production pipelines must be established, combined with tangential flow filtration and optimized loading techniques to achieve high-purity exosomes with consistent batch quality[55]. From a pharmacokinetic perspective, in vivo fluorescence imaging is required to systematically characterize the distribution, accumulation and clearance profiles of modified and unmodified exosomes, quantifying the influence of peptide modification on native organ homing properties. Safety assessments should adhere to GLP guidelines, with gradient-dose and long-term repeated administration protocols to evaluate systemic and kidney-specific toxicity, focusing on immunogenicity and chronic organ damage risks[56].

Based on our current findings, multiple testable directions can be pursued in follow-up research: in vivo near-infrared fluorescence imaging to quantify the renal enrichment advantage

afforded by Cyclo(RGDfC); supplementary control groups to dissect individual functions of each carrier component and optimize conjugation and loading protocols; integrated multi-omics alongside molecular interaction assays to delineate the complete HBx-FOSB upstream and downstream signaling cascade; standardized exosome preparation and quality control platforms coupled with long-term safety evaluation in large animals, as well as exploration of combinatorial therapy with clinical anti-HBV agents. Furthermore, the Cyclo(RGDfC) modification strategy established herein exhibits broad translational potential, adaptable to the development of targeted nanocarriers for other glomerulopathies featuring podocyte injury such as IgA nephropathy and diabetic kidney disease.

Collectively, integrated evidence from clinical renal biopsy transcriptomics, in vitro cellular functional assays and in vivo intervention in HBx transgenic mice supports two core innovations of this work. First, clinical specimen-based transcriptomic screening for the first time identifies FOSB as a master transcriptional regulator mediating HBx-induced podocyte injury, establishing a novel HBx-FOSB pathogenic axis that enriches the molecular mechanistic landscape of HBV-GN. Second, we innovatively engineered Cyclo(RGDfC)-conjugated BMSC exosomes loaded with FOSB siRNA, overcoming the inherent deficiencies of native exosomes including poor renal tropism and low nucleic acid loading capacity to achieve specific gene silencing in injured podocytes. Consistent in vitro and in vivo data demonstrate that this delivery system robustly inhibits podocyte apoptosis, aberrant invasion and chronic inflammatory infiltration, ameliorating renal pathological lesions and restoring renal function. Relative to conventional immunosuppressive regimens and viral gene vectors, this cell-free carrier confers superior safety profiles and allows prolonged intervention, offering an original experimental framework for precision RNA interference therapy against HBV-GN. The modified exosome platform also provides a referenceable engineering paradigm for targeted nanomedicine development across all podocyte-dominant glomerular disorders, bearing significant implications for basic nephrological research and clinical translational advancement.

Data availability statement

The datasets presented in this study can be found in online repositories. The names of the repository/repositories and accession number(s) can be found in the article/Supplementary Material.

Funding

The author(s) declare financial support was received for the research, authorship, and/or publication of this article. This work was supported by the National Natural Science Foundation of China (grant number NSFC 82370724) and Qingdao Key Health Discipline Development Fund and Qingdao Key Clinical Specialty Elite Discipline.

Conflict of interest

The authors declare that the research was conducted in the absence of any commercial or financial relationships that could be construed as a potential conflict of interest.

Publisher’s note

All claims expressed in this article are solely those of the authors and do not necessarily represent those of their affiliated organizations, or those of the publisher, the editors and the reviewers. Any product that may be evaluated in this article, or claim that may be made by its manufacturer, is not guaranteed or endorsed by the publisher.

References

[1] Global, regional, and national burden of hepatitis B, 1990-2019: a systematic analysis for the Global Burden of Disease Study 2019 [J]. Lancet Gastroenterol Hepatol, 2022, 7(9): 796-829.

[2] CACOUB P, ASSELAH T. Hepatitis B Virus Infection and Extra-Hepatic Manifestations: A Systemic Disease [J]. Am J Gastroenterol, 2022, 117(2): 253-63.

[3] HU Y, ZHANG Y, JIANG W. Targeting hepatitis B virus-associated nephropathy: efficacy and challenges of current antiviral treatments [J]. Clin Exp Med, 2025, 25(1): 57.

[4] HE P, ZHANG D, LI H, et al. Hepatitis B virus X protein modulates apoptosis in human renal proximal tubular epithelial cells by activating the JAK2/STAT3 signaling pathway [J]. Int J Mol Med, 2013, 31(5): 1017-29.

[5] HERRSCHER C, ROINGEARD P, BLANCHARD E. Hepatitis B Virus Entry into Cells [J]. Cells, 2020, 9(6).

[6] ZHAO F, XIE X, TAN X, et al. The Functions of Hepatitis B Virus Encoding Proteins: Viral Persistence and Liver Pathogenesis [J]. Front Immunol, 2021, 12: 691766.

[7] YOU H, QIN S, ZHANG F, et al. Regulation of Pattern-Recognition Receptor Signaling by HBX During Hepatitis B Virus Infection [J]. Front Immunol, 2022, 13: 829923.

[8] HAN W, LUO M, HE M, et al. HBx gene transfection affects the cycle of primary renal tubular epithelial cells through regulating cyclin expression [J]. Mol Med Rep, 2018, 18(2): 1947-54.

[9] ZHANG Y, CHEN Y, YANG F, et al. HBx transfection limits proliferative capacity of podocytes through cell cycle regulation [J]. Acta Biochim Biophys Sin (Shanghai), 2014, 46(12): 1016-23.

[10] LI M, HU L, ZHU F, et al. Hepatitis B virus X protein promotes renal epithelial-mesenchymal transition in human renal proximal tubule epithelial cells through the activation of NF-κB [J]. Int J Mol Med, 2016, 38(2): 513-20.

[11] KLINGEMANN H, MATZILEVICH D, MARCHAND J. Mesenchymal Stem Cells - Sources and Clinical Applications [J]. Transfus Med Hemother, 2008, 35(4): 272-7.

[12] KALLURI R. The biology and function of exosomes in cancer [J]. J Clin Invest, 2016, 126(4): 1208-15.

[13] LI B, QI C, ZHANG Y, et al. Frontier role of extracellular vesicles in kidney disease [J]. J Nanobiotechnology, 2024, 22(1): 583.

[14] CECCOTTI E, QUAGLIA M, CAMUSSI G, et al. Mesenchymal stem cells derived extracellular vesicles for chronic kidney disease: pleiotropic mechanisms of actions of a versatile therapy [J]. Front Bioeng Biotechnol, 2025, 13: 1612193.

[15] WANG Y, GUO Y F, FU G P, et al. Protective effect of miRNA-containing extracellular vesicles derived from mesenchymal stromal cells of old rats on renal function in chronic kidney disease [J]. Stem Cell Res Ther, 2020, 11(1): 274.

[16] HUANG L, WU E, LIAO J, et al. Research Advances of Engineered Exosomes as Drug Delivery Carrier [J]. ACS Omega, 2023, 8(46): 43374-87.

[17] WANG C, SHEN Z, CHEN Y, et al. Research Progress on Cyclic-Peptide Functionalized Nanoparticles for Tumor-Penetrating Delivery [J]. Int J Nanomedicine, 2024, 19: 12633-52.

[18] POLLINGER K, HENNIG R, BREUNIG M, et al. Kidney podocytes as specific targets for cyclo(RGDfC)-modified nanoparticles [J]. Small, 2012, 8(21): 3368-75.

[19] MARELLI U K, RECHENMACHER F, SOBAHI T R, et al. Tumor Targeting via Integrin Ligands [J]. Front Oncol, 2013, 3: 222.

[20] ZHOU J, LI R, ZHANG J, et al. Targeting Interstitial Myofibroblast-Expressed Integrin αvβ3 Alleviates Renal Fibrosis [J]. Mol Pharm, 2021, 18(3): 1373-85.

[21] RAVAL N, JOGI H, GONDALIYA P, et al. Cyclo-RGD Truncated Polymeric Nanoconstruct with Dendrimeric Templates for Targeted HDAC4 Gene Silencing in a Diabetic Nephropathy Mouse Model [J]. Mol Pharm, 2021, 18(2): 641-66.

[22] LIN Z, ZHANG X, LAI Y, et al. Glomerulonephritis, the Most Common Extrahepatic Manifestation Caused by Hepatitis B Virus Infection: Possible Pathogenesis and Therapeutic Approaches [J]. J Med Virol, 2025, 97(12): e70731.

[23] SONGTANIN B, CHAISRIMANEEPAN N, MENDóZA R, et al. Burden, Outcome, and Comorbidities of Extrahepatic Manifestations in Hepatitis B Virus Infections [J]. Viruses, 2024, 16(4).

[24] HE Z, ZHU Y, NIU Y, et al. HBx promotes podocyte-macrophage transdifferentiation by mediating NLRP3 expression in hepatitis B virus-associated glomerulonephritis [J]. Virol J, 2025, 22(1): 301.

[25] MANN N, SUN H, MAJMUNDAR A J. Mechanisms of podocyte injury in genetic kidney disease [J]. Pediatr Nephrol, 2025, 40(5): 1523-38.

[26] CUNANAN J, ZHANG D, PEIRED A J, et al. Podocytes in health and glomerular disease [J]. Front Cell Dev Biol, 2025, 13: 1564847.

[27] AGUSTININGSIH A, RASYAK M R, TURYADI, et al. The oncogenic role of hepatitis B virus X gene in hepatocarcinogenesis: recent updates [J]. Explor Target Antitumor Ther, 2024, 5(1): 120-34.

[28] SCHOLLMEIER A, GLITSCHER M, HILDT E. Relevance of HBx for Hepatitis B Virus-Associated Pathogenesis [J]. Int J Mol Sci, 2023, 24(5).

[29] CORDIER F, CREYTENS D. New kids on the block: FOS and FOSB gene [J]. J Clin Pathol, 2023, 76(11): 721-6.

[30] TANG X, SHEN C, LIU C, et al. Network expression analysis identifies and experimentally validates the involvement of Fosb in acute kidney injury [J]. FASEB Bioadv, 2025, 7(4): e70002.

[31] YU X, WANG Y, SONG Y, et al. AP-1 is a regulatory transcription factor of inflammaging in the murine kidney and liver [J]. Aging Cell, 2023, 22(7): e13858.

[32] NESTLER E J. ΔFosB: a transcriptional regulator of stress and antidepressant responses [J]. Eur J Pharmacol, 2015, 753: 66-72.

[33] PARK H J, KIM J W, CHO B S, et al. Association of FOS-like antigen 1 promoter polymorphism with podocyte foot process effacement in immunoglobulin A nephropathy patients [J]. J Clin Lab Anal, 2014, 28(5): 391-7.

[34] HOWE B M, BRUNO S B, HIGGS K A, et al. FosB expression in the central nervous system following isotonic volume expansion in unanesthetized rats [J]. Exp Neurol, 2004, 187(1): 190-8.

[35] LIAO Y, WANG Z, WANG L, et al. MicroRNA-27a-3p directly targets FosB to regulate cell proliferation, apoptosis, and inflammation responses in immunoglobulin a nephropathy [J]. Biochem Biophys Res Commun, 2020, 529(4): 1124-30.

[36] MUSTAFA M, AHMAD R, TANTRY I Q, et al. Apoptosis: A Comprehensive Overview of Signaling Pathways, Morphological Changes, and Physiological Significance and Therapeutic Implications [J]. Cells, 2024, 13(22).

[37] QIAN S, LONG Y, TAN G, et al. Programmed cell death: molecular mechanisms, biological functions, diseases, and therapeutic targets [J]. MedComm (2020), 2024, 5(12): e70024.

[38] PFEFFER C M, SINGH A T K. Apoptosis: A Target for Anticancer Therapy [J]. Int J Mol Sci, 2018, 19(2).

[39] SZEGEZDI E, LOGUE S E, GORMAN A M, et al. Mediators of endoplasmic reticulum stress-induced apoptosis [J]. EMBO Rep, 2006, 7(9): 880-5.

[40] KIM H J, KIM S Y, KIM J, et al. Hepatitis B virus X protein induces apoptosis by enhancing translocation of Bax to mitochondria [J]. IUBMB Life, 2008, 60(7): 473-80.

[41] DJIADEU P, KOTRA L P, SWEEZEY N, et al. Surfactant protein D delays Fas- and TRAIL-mediated extrinsic pathway of apoptosis in T cells [J]. Apoptosis, 2017, 22(5): 730-40.

[42] RADISKY E S. Extracellular proteolysis in cancer: Proteases, substrates, and mechanisms in tumor progression and metastasis [J]. J Biol Chem, 2024, 300(6): 107347.

[43] KUROSAKA S, KASHINA A. Cell biology of embryonic migration [J]. Birth Defects Res C Embryo Today, 2008, 84(2): 102-22.

[44] NIU D, YANG J J, HE D F. The role of macrophages in renal fibrosis and therapeutic prospects [J]. PeerJ, 2025, 13: e19769.

[45] JIANG H, SHEN Z, ZHUANG J, et al. Understanding the podocyte immune responses in proteinuric kidney diseases: from pathogenesis to therapy [J]. Front Immunol, 2023, 14: 1335936.

[46] GUITERAS R, FLAQUER M, CRUZADO J M. Macrophage in chronic kidney disease [J]. Clin Kidney J, 2016, 9(6): 765-71.

[47] PENG W, PEI G Q, TANG Y, et al. IgA1 deposition may induce NLRP3 expression and macrophage transdifferentiation of podocyte in IgA nephropathy [J]. J Transl Med, 2019, 17(1): 406.

[48] LIU Z J, ZHUGE Y, VELAZQUEZ O C. Trafficking and differentiation of mesenchymal stem cells [J]. J Cell Biochem, 2009, 106(6): 984-91.

[49] YIN K, WANG S, ZHAO R C. Exosomes from mesenchymal stem/stromal cells: a new therapeutic paradigm [J]. Biomark Res, 2019, 7: 8.

[50] ZHANG T, ZHANG L, MA X, et al. The tiny giants of regeneration: MSC-derived extracellular vesicles as next-generation therapeutics [J]. Frontiers in Cell and Developmental Biology, 2025, Volume 13 - 2025.

[51] DU Y, LIU D, LIU J, et al. Exosomes as Emerging Nanocarriers for Targeted Cancer Therapy [J]. Int J Nanomedicine, 2026, 21: 585042.

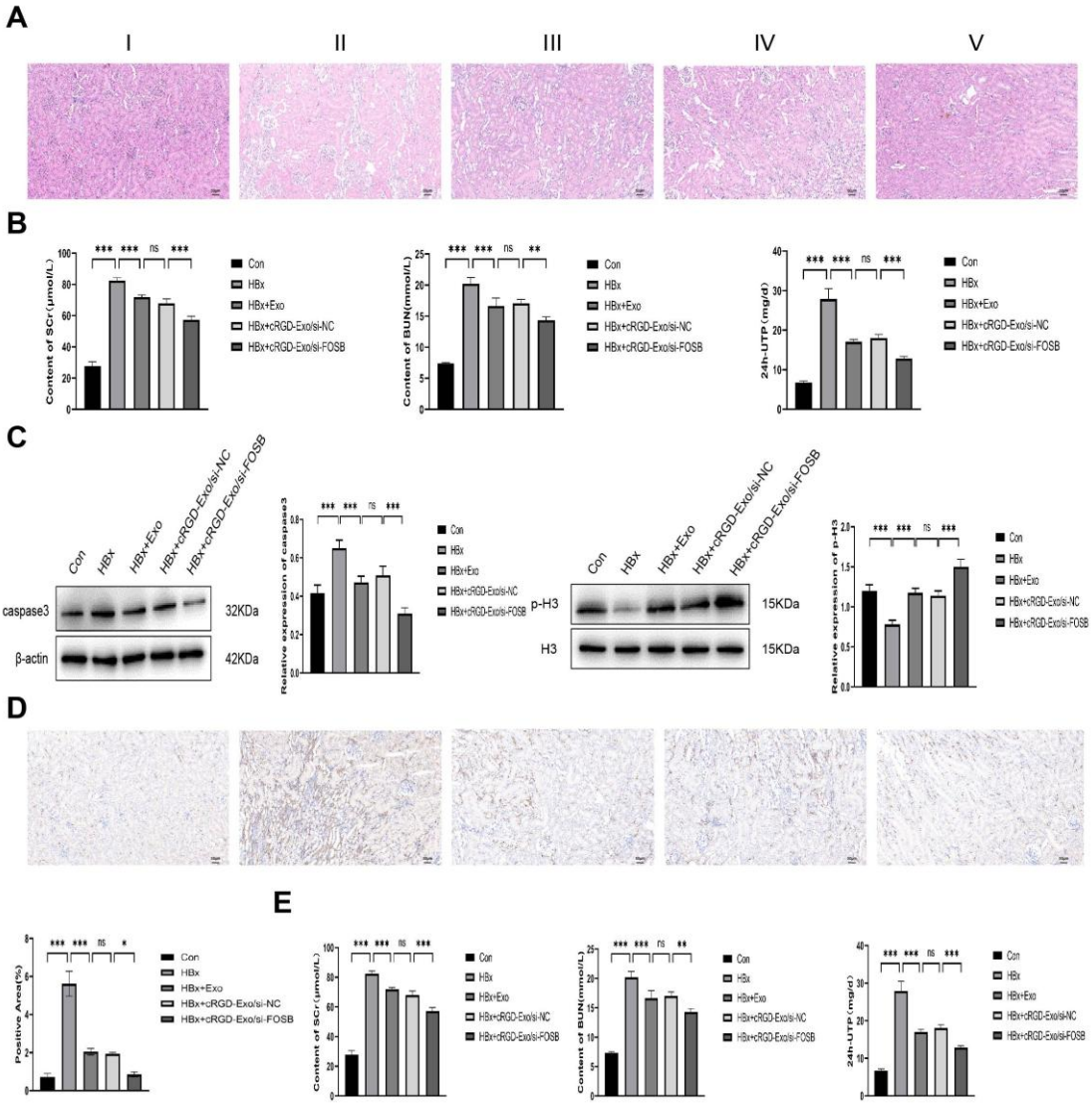
[52] KANG M, JORDAN V, BLENKIRON C, et al. Biodistribution of extracellular vesicles following administration into animals: A systematic review [J]. J Extracell Vesicles, 2021, 10(8): e12085.

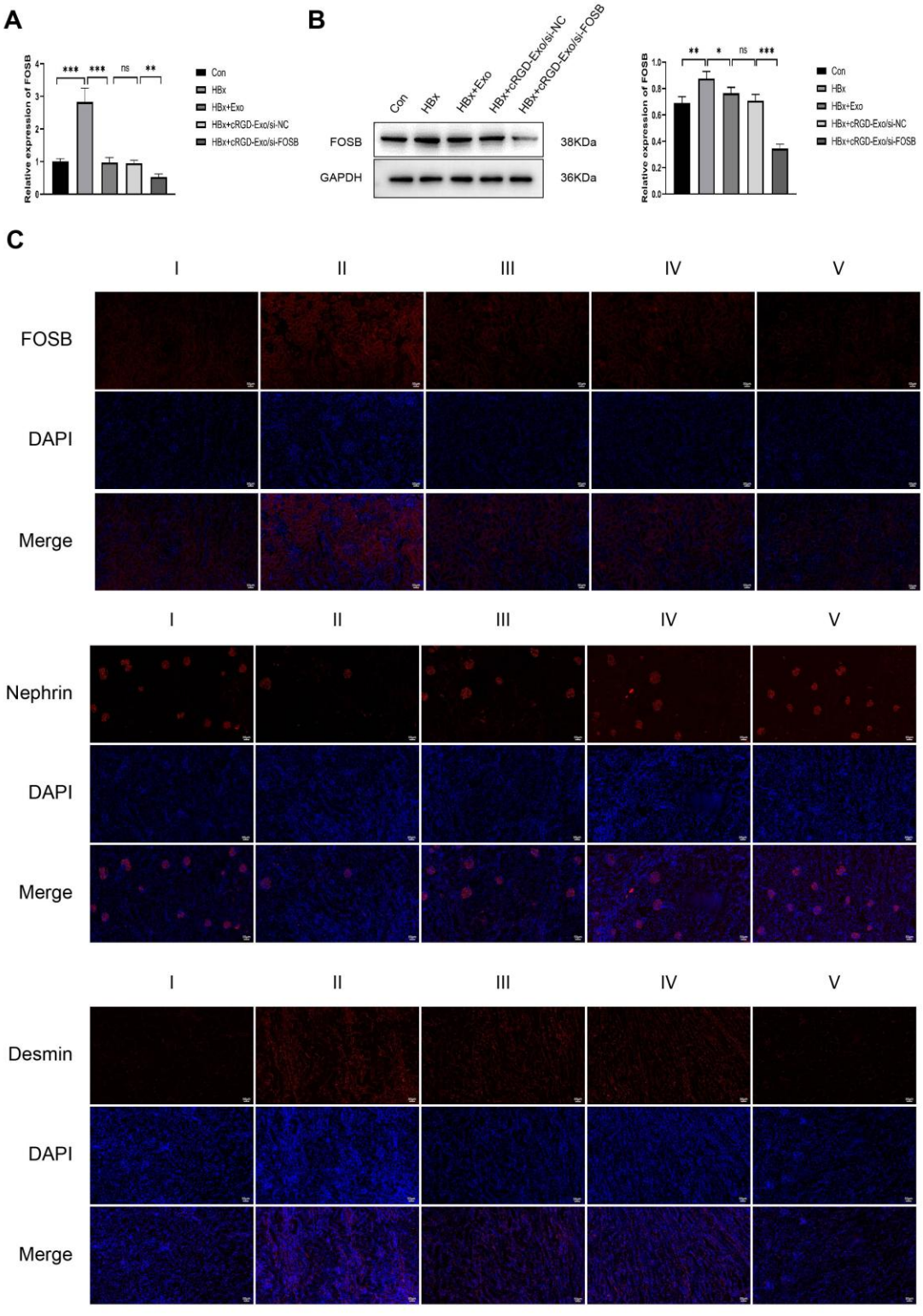
[53] TRIMARCHI H, ORTIZ A, SáNCHEZ-NIñO M D. Lyso-Gb3 Increases αvβ3 Integrin Gene Expression in Cultured Human Podocytes in Fabry Nephropathy [J]. J Clin Med, 2020, 9(11).

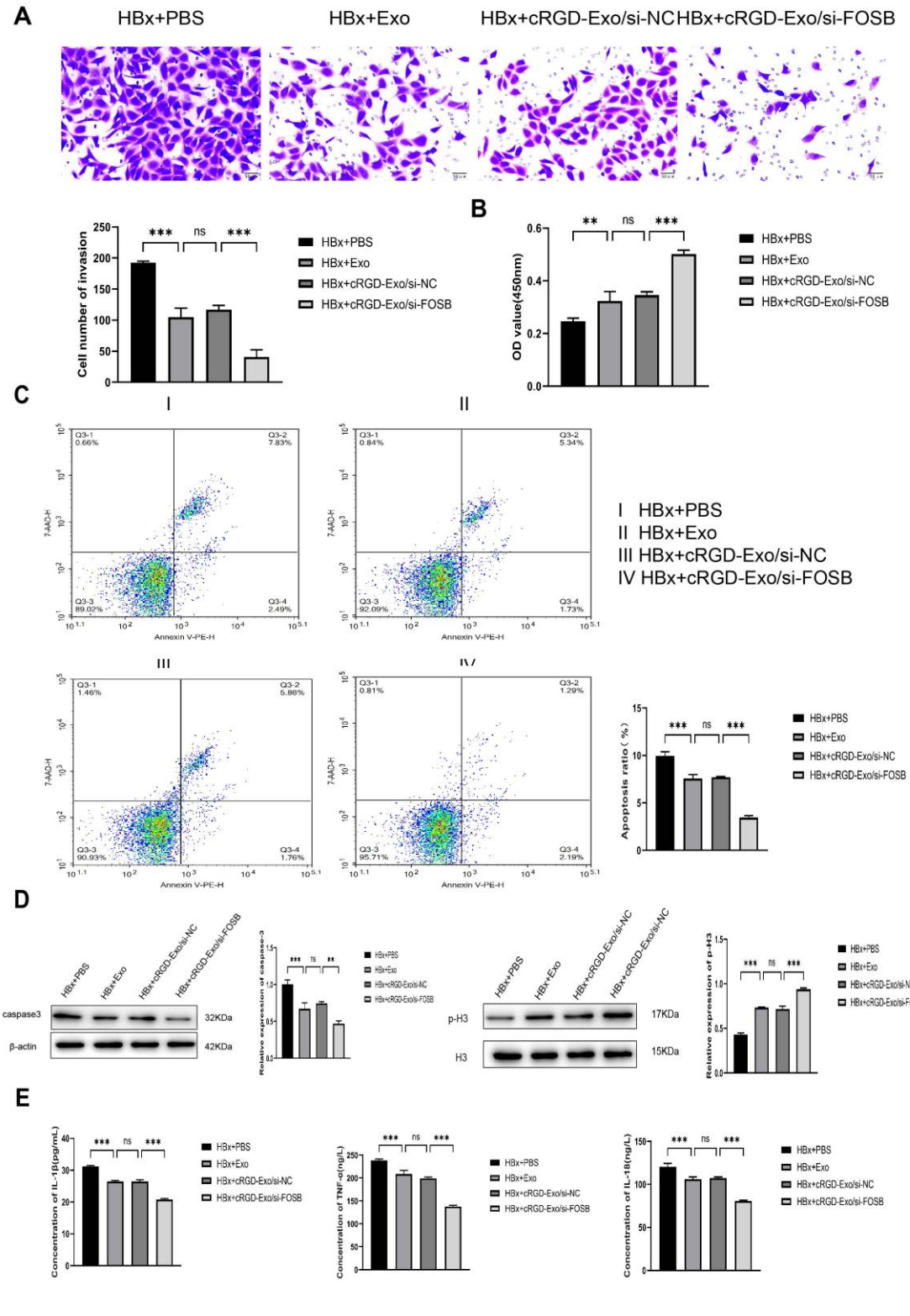
[54] TAN Z, HU Y, WU Y, et al. Kidney-targeted drug delivery: from physiological mechanisms to precision therapeutics [J]. Front Bioeng Biotechnol, 2026, 14: 1763546.

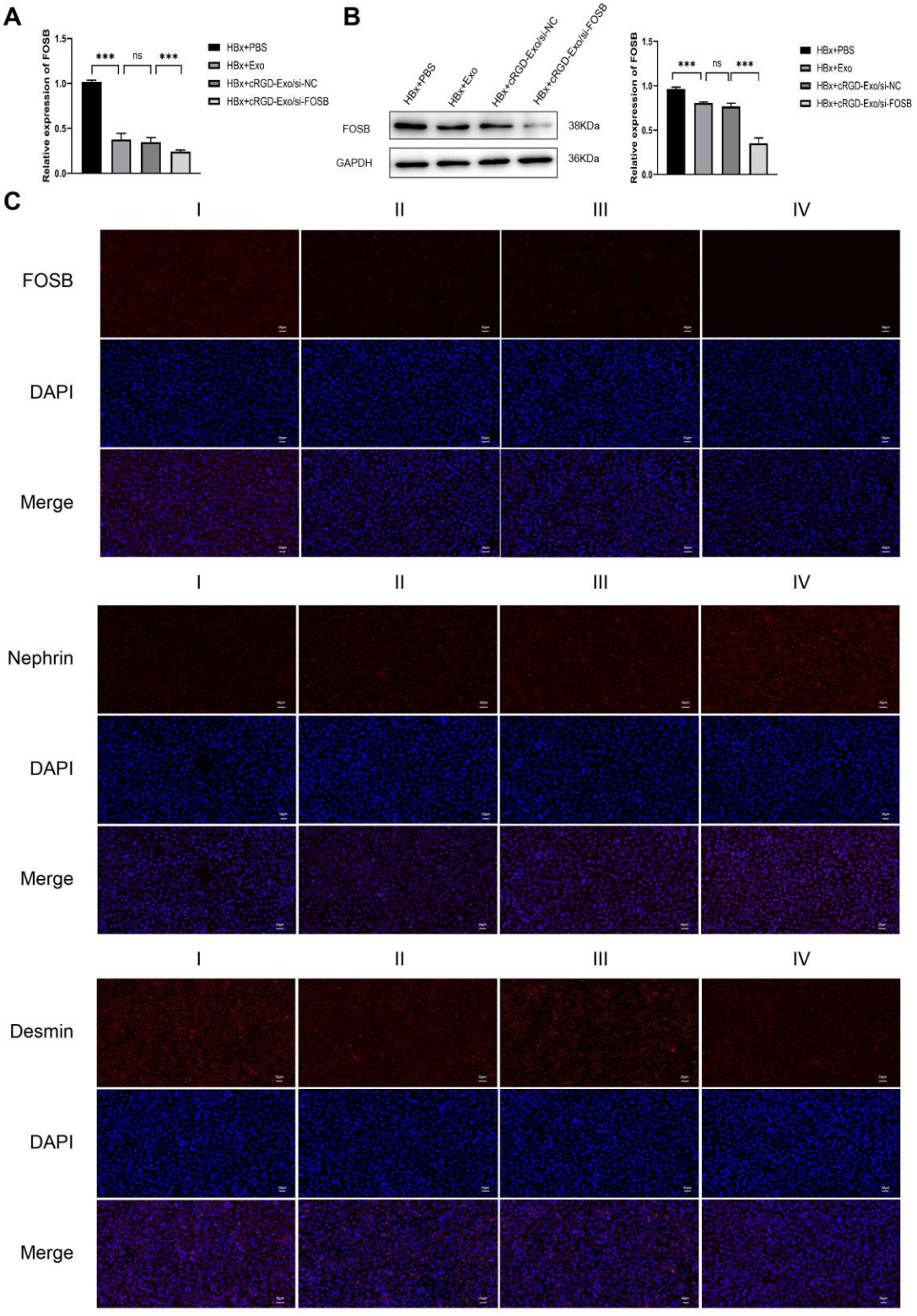
[55] HUMBERT C, CORDIER C, DRUT I, et al. GMP-Compliant Process for the Manufacturing of an Extracellular Vesicles-Enriched Secretome Product Derived From Cardiovascular Progenitor Cells Suitable for a Phase I Clinical Trial [J]. J Extracell Vesicles, 2025, 14(8): e70145.

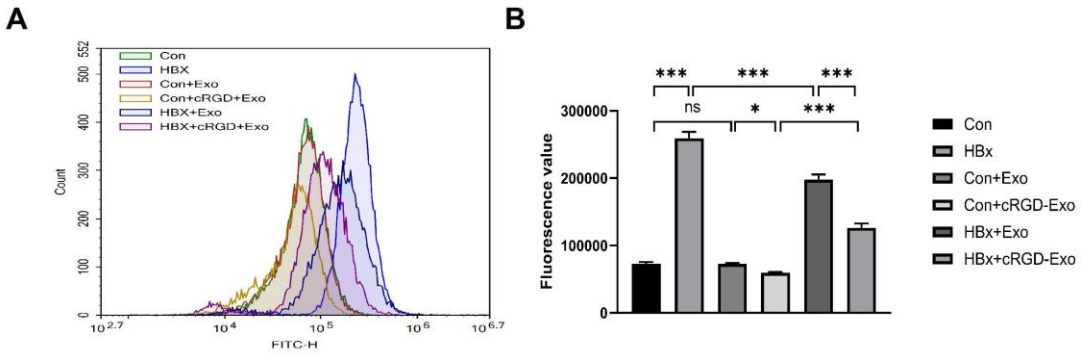
[56] YOO M H, LEE A R, MOON K S. Characteristics of Extracellular Vesicles and Preclinical Testing Considerations Prior to Clinical Applications [J]. Biomedicines, 2022, 10(4).

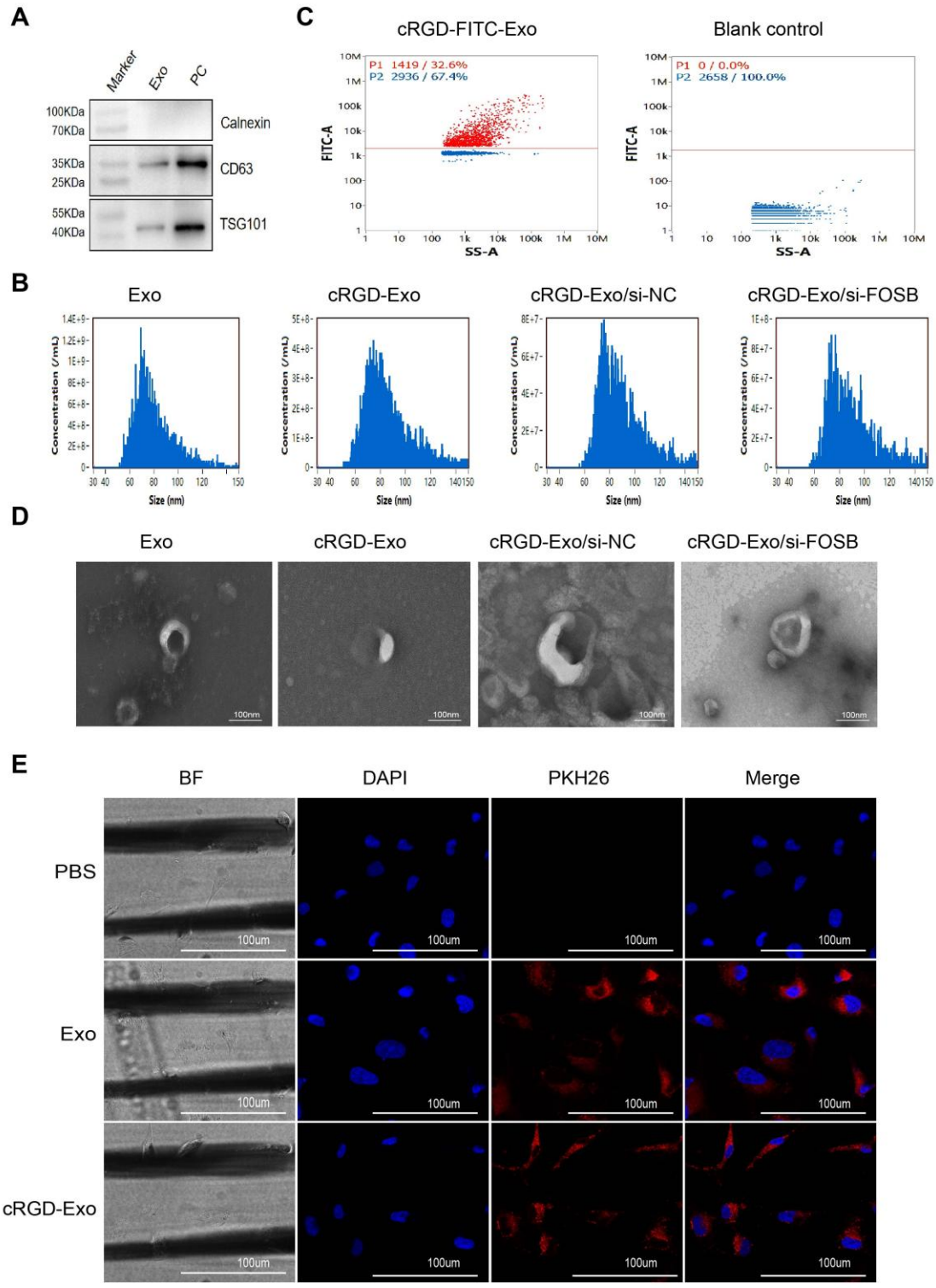

A
I
II
III
IV
V
B
Content of SCr (μmol/L)
Content of BUN(mmol/L)
24h-UTP (mg/d)
Con
HBx
HBx+Exo
HBx+cRGD-Exo/si-NC
HBx+cRGD-Exo/si-FOSB
C
Con
HBx
HBx+Exo
HBx+cRGD-Exo/si-NC
HBx+cRGD-Exo/si-FOSB
caspase3
32KDa
β-actin
42KDa
Relative expression of caspase3
p-H3
15KDa
H3
15KDa
Relative expression of p-H3
D
E
Positive Area(%)
Content of SCr (μmol/L)
Content of BUN(mmol/L)
24h-UTP (mg/d)

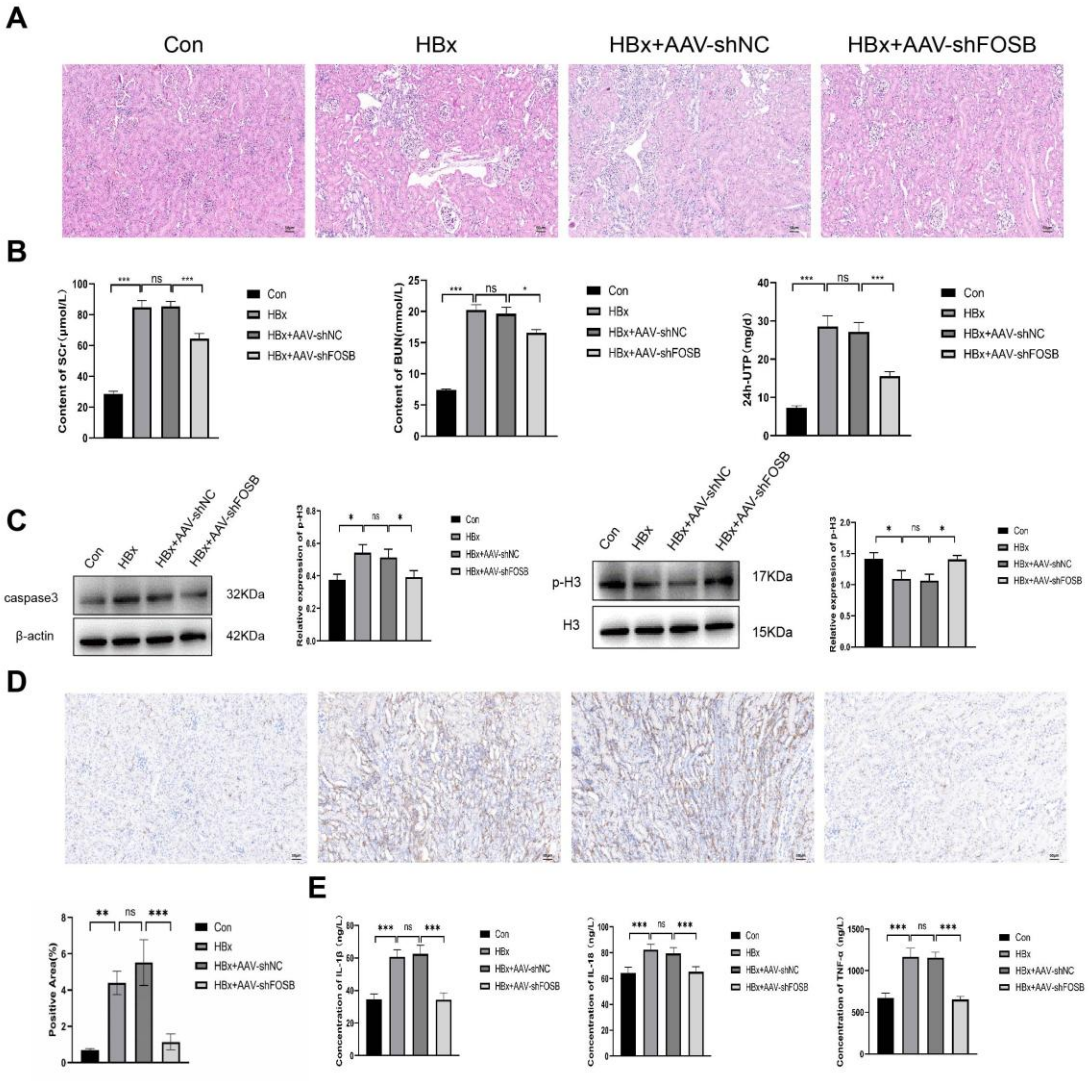

A
Relative expression of FOSB
***
***
ns
**
Con
HBx
HBx+Exo
HBx+cRGD-Exo/si-NC
HBx+cRGD-Exo/si-FOSB
B
Con
HBx
HBx+Exo
HBx+cRGD-Exo/si-NC
HBx+cRGD-Exo/si-FOSB
FOSB
38KDa
GAPDH
36KDa
Relative expression of FOSB
**
*
ns
***
C
I
II
III
IV
V
FOSB
DAPI
Merge
Nephrin
Desmin

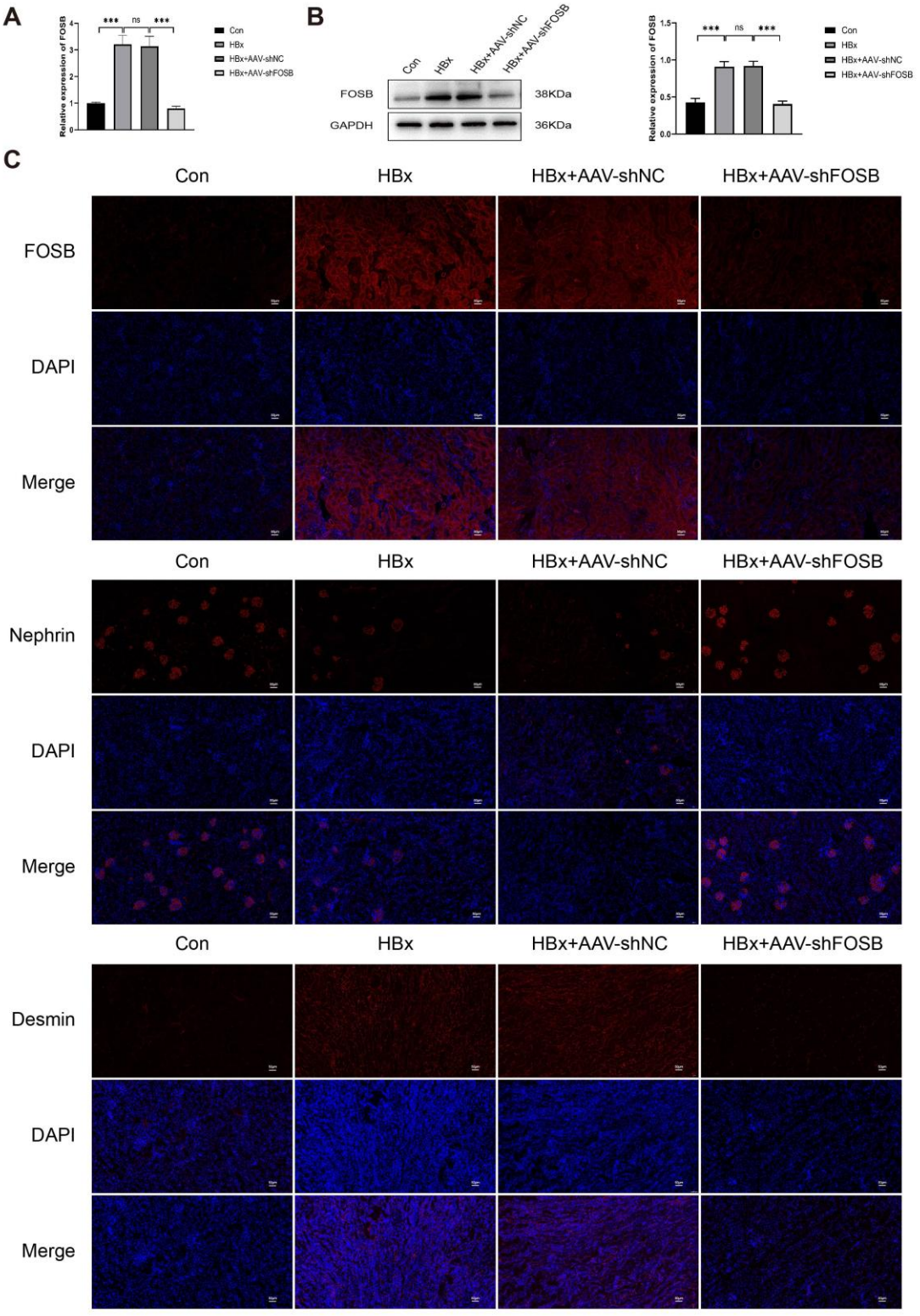

A
HBx+PBS
HBx+Exo
HBx+cRGD-Exo/si-NC
HBx+cRGD-Exo/si-FOSB
Cell number of invasion
B
OD value(450nm)
C
I HBx+PBS
II HBx+Exo
III HBx+cRGD-Exo/si-NC
IV HBx+cRGD-Exo/si-FOSB
Annexin V-PE-H
7-AAD-H
Apoptosis ratio (%)
D
caspase3
β-actin
32KDa
42KDa
Relative expression of caspase-3
p-H3
H3
17KDa
15KDa
Relative expression of p-H3
E
Concentration of IL-1β(pg/mL)
Concentration of TNF-α(ng/L)
Concentration of IL-18(ng/L)

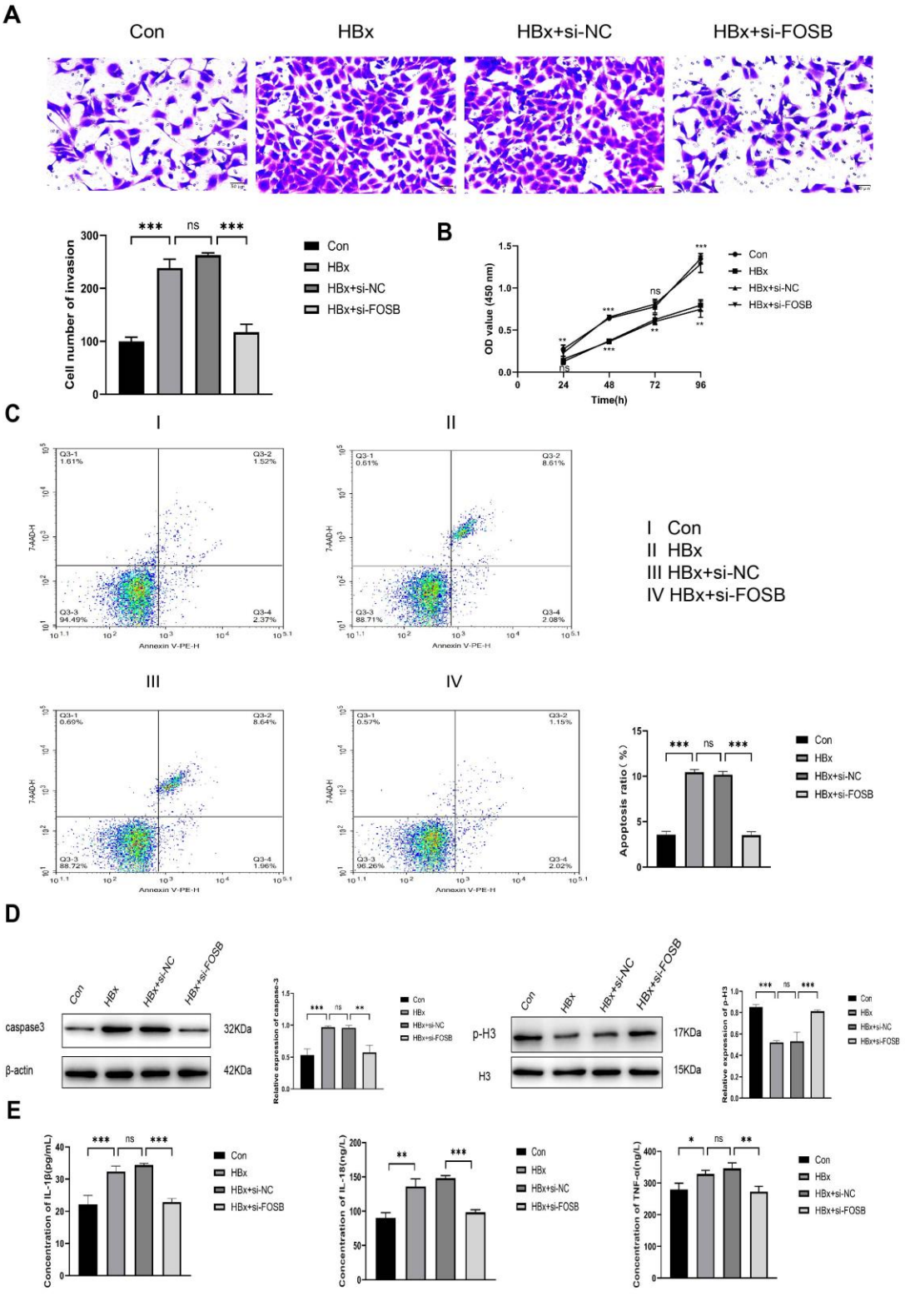

A
Relative expression of FOSB
1.5
1.0
0.5
0.0
***
ns
***
HBx+PBS
HBx+Exo
HBx+cRGD-Exo/si-NC
HBx+cRGD-Exo/si-FOSB
B
HBx+PBS
HBx+Exo
HBx+cRGD-Exo/si-NC
HBx+cRGD-Exo/si-FOSB
FOSB
38KDa
GAPDH
36KDa
Relative expression of FOSB
1.5
1.0
0.5
0.0
***
ns
***
HBx+PBS
HBx+Exo
HBx+cRGD-Exo/si-NC
HBx+cRGD-Exo/si-FOSB
C
I
II
III
IV
FOSB
DAPI
Merge
I
II
III
IV
Nephrin
DAPI
Merge
I
II
III
IV
Desmin
DAPI
Merge

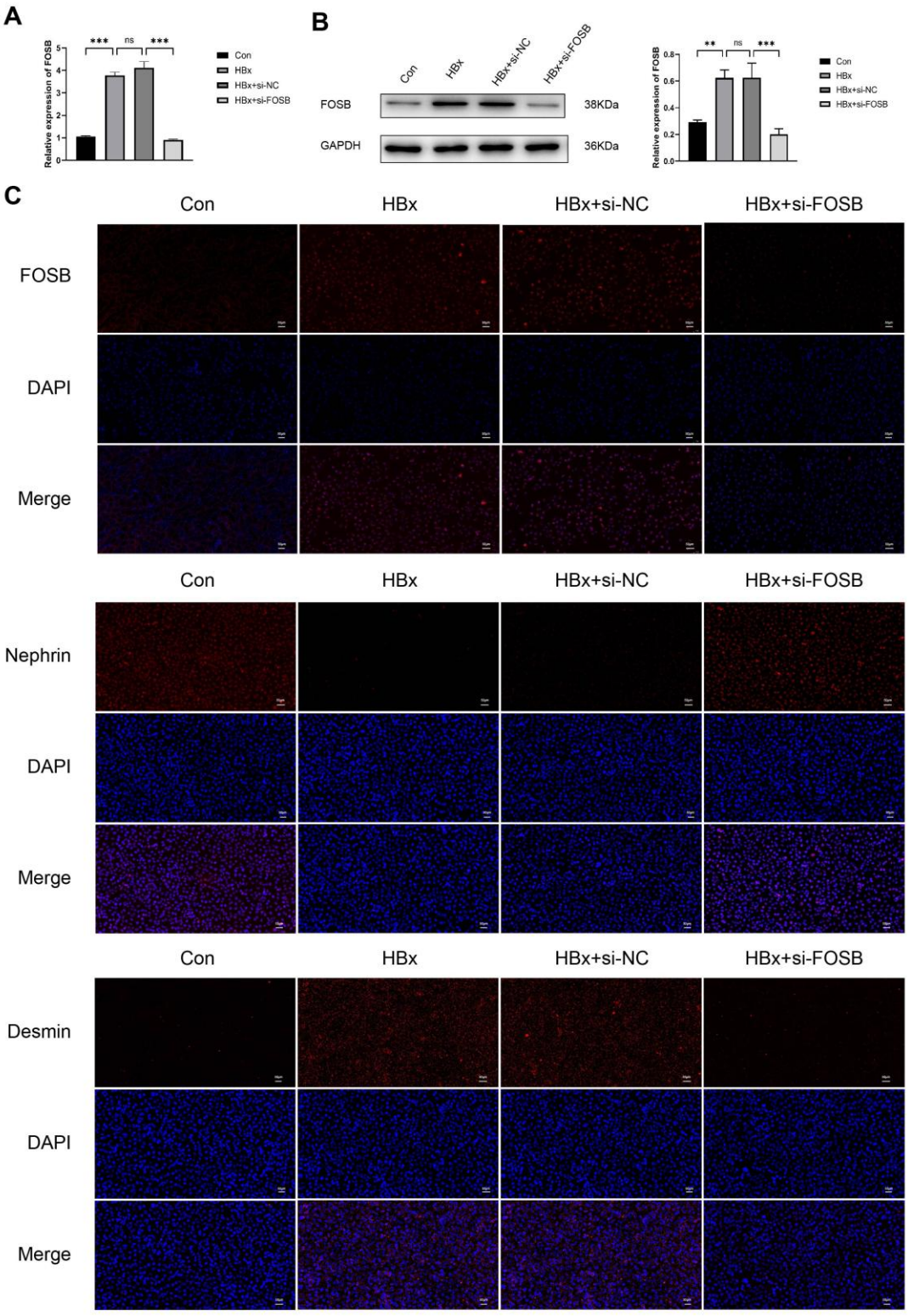

A
Con
HBX
Con+Exo
Con+cRGD+Exo
HBX+Exo
HBX+cRGD+Exo
Count
FITC-H
B
Fluorescence value
300000
200000
100000
0
***
***
***
ns
*
***
Con
HBx
Con+Exo
Con+cRGD-Exo
HBx+Exo
HBx+cRGD-Exo

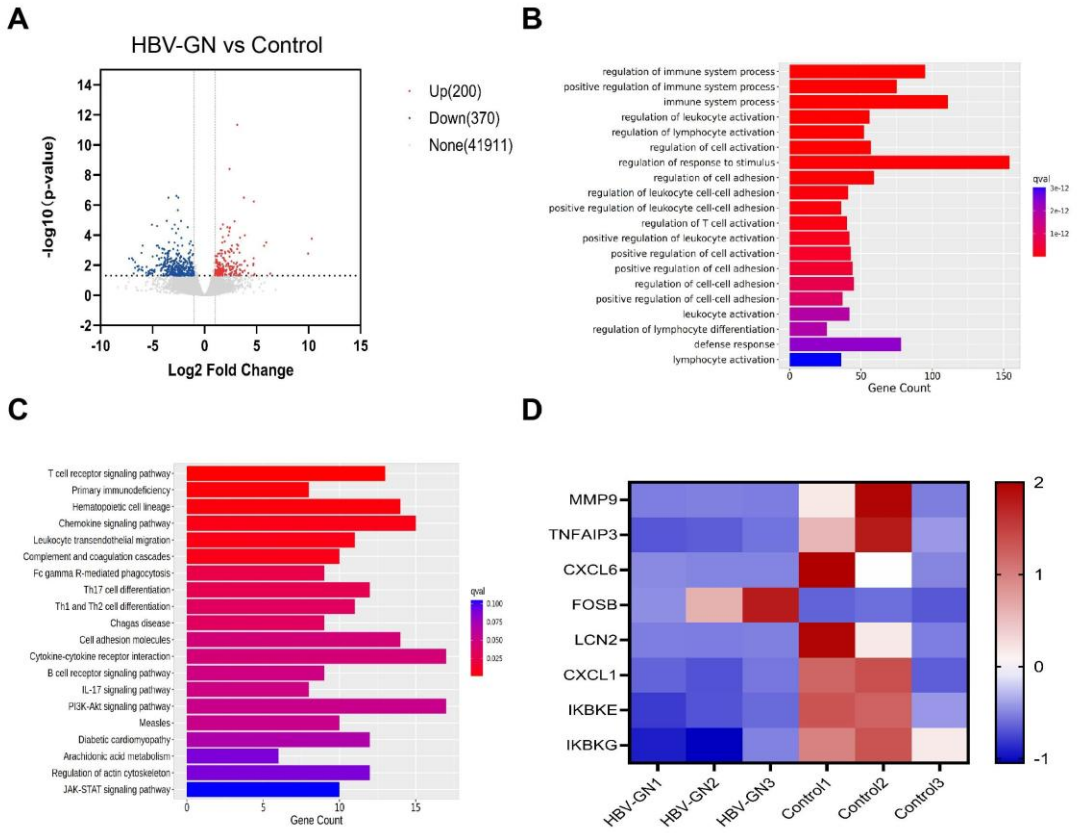

A
Marker
Exo
PC
100KDa
70KDa
Calnexin
35KDa
25KDa
CD63
55KDa
40KDa
TSG101
C
cRGD-FITC-Exo
Blank control
P1 1419 / 32.6%
P2 2936 / 67.4%
P1 0 / 0.0%
P2 2658 / 100.0%
FITC-A
SS-A
B
Exo
cRGD-Exo
cRGD-Exo/si-NC
cRGD-Exo/si-FOSB
Concentration (/mL)
Size (nm)
D
Exo
cRGD-Exo
cRGD-Exo/si-NC
cRGD-Exo/si-FOSB
100nm
E
BF
DAPI
PKH26
Merge
PBS
Exo
cRGD-Exo
100um


A
Con
HBx
HBx+AAV-shNC
HBx+AAV-shFOSB
B
Content of SCr (μmol/L)
Content of BUN(mmol/L)
24h-UTP (mg/d)
Con
HBx
HBx+AAV-shNC
HBx+AAV-shFOSB
C
caspase3
β-actin
32KDa
42KDa
p-H3
H3
17KDa
15KDa
Relative expression of p-H3
D
E
Positive Area(%)
Concentration of IL-1β (ng/L)
Concentration of IL-18 (ng/L)
Concentration of TNF-α (ng/L)


A
Relative expression of FOSB
***
ns
***
Con
HBx
HBx+AAV-shNC
HBx+AAV-shFOSB
B
Con
HBx
HBx+AAV-shNC
HBx+AAV-shFOSB
FOSB
38KDa
GAPDH
36KDa
Relative expression of FOSB
***
ns
***
Con
HBx
HBx+AAV-shNC
HBx+AAV-shFOSB
C
Con
HBx
HBx+AAV-shNC
HBx+AAV-shFOSB
FOSB
DAPI
Merge
Con
HBx
HBx+AAV-shNC
HBx+AAV-shFOSB
Nephrin
DAPI
Merge
Con
HBx
HBx+AAV-shNC
HBx+AAV-shFOSB
Desmin
DAPI
Merge


A
Con
HBx
HBx+si-NC
HBx+si-FOSB
Cell number of invasion
***
ns
***
B
OD value (450 nm)
Time(h)
C
I
II
III
IV
7-AAD-H
Annexin V-PE-H
I Con
II HBx
III HBx+si-NC
IV HBx+si-FOSB
Apoptosis ratio (%)
D
caspase3
β-actin
32KDa
42KDa
Relative expression of caspase-3
p-H3
H3
17KDa
15KDa
Relative expression of p-H3
E
Concentration of IL-1β(pg/mL)
Concentration of IL-18(ng/L)
Concentration of TNF-α(ng/L)


A
Relative expression of FOSB
***
ns
***
Con
HBx
HBx+si-NC
HBx+si-FOSB
B
Con
HBx
HBx+si-NC
HBx+si-FOSB
FOSB
38KDa
GAPDH
36KDa
Relative expression of FOSB
**
ns
***
C
Con
HBx
HBx+si-NC
HBx+si-FOSB
FOSB
DAPI
Merge
Nephrin
Desmin


A
HBV-GN vs Control
-log10 (p-value)
Log2 Fold Change
Up(200)
Down(370)
None(41911)
B
regulation of immune system process
positive regulation of immune system process
immune system process
regulation of leukocyte activation
regulation of lymphocyte activation
regulation of cell activation
regulation of response to stimulus
regulation of cell adhesion
regulation of leukocyte cell-cell adhesion
positive regulation of leukocyte cell-cell adhesion
regulation of T cell activation
positive regulation of leukocyte activation
positive regulation of cell activation
positive regulation of cell adhesion
regulation of cell-cell adhesion
positive regulation of cell-cell adhesion
leukocyte activation
regulation of lymphocyte differentiation
defense response
lymphocyte activation
Gene Count
qval
C
T cell receptor signaling pathway
Primary immunodeficiency
Hematopoietic cell lineage
Chemokine signaling pathway
Leukocyte transendothelial migration
Complement and coagulation cascades
Fc gamma R-mediated phagocytosis
Th17 cell differentiation
Th1 and Th2 cell differentiation
Chagas disease
Cell adhesion molecules
Cytokine-cytokine receptor interaction
B cell receptor signaling pathway
IL-17 signaling pathway
PI3K-Akt signaling pathway
Measles
Diabetic cardiomyopathy
Arachidonic acid metabolism
Regulation of actin cytoskeleton
JAK-STAT signaling pathway
Gene Count
qval
D
MMP9
TNFAIP3
CXCL6
FOSB
LCN2
CXCL1
IKBKE
IKBKG
HBV-GN1
HBV-GN2
HBV-GN3
Control1
Control2
Control3

Supplementary Files

This is a list of supplementary files associated with this preprint. Click to download.

- Supplementarymaterial.docx